Title: Asymmetric histone incorporation during DNA replication in *Drosophila* male germline stem cells

Authors: Matthew Wooten[1], Jonathan Snedeker[*,1], Zehra Nizami[*,2], Xinxing Yang[*,3], Elizabeth Urban[1], Ashlee Feng[1], Jee Min Kim[1], Joseph Gall[2], Jie Xiao[3], Xin Chen[1,#]

*: equal contribution

[#]: Correspondence to: Xin Chen, Ph.D., Department of Biology, 3400 North Charles Street, The Johns Hopkins University, Baltimore, MD 21218-2685, USA. Tel: 410-516-4576; Fax: 410-516-5213; Email: xchen32@jhu.edu

Affiliations:

[1] Department of Biology, The Johns Hopkins University, Baltimore, MD 21218, USA

[2] Carnegie Institution for Science, Department of Embryology, Baltimore, MD 21218, USA

[3] Department of Biophysics and Biophysical Chemistry, Johns Hopkins University School of Medicine, Baltimore, MD 21205, USA

Running Title: DNA replication establishes asymmetric epigenomes

SUMMARY

Many stem cells undergo asymmetric division to produce both a self-renewing stem cell and a differentiating daughter cell. We previously reported that in male *Drosophila* germline stem cells (GSCs), preexisting (old) histone H3 is inherited to the self-renewed stem cell, whereas the differentiating daughter is enriched with newly synthesized (new) H3. However, the molecular mechanisms that establish asymmetric H3 distribution on sister chromatids were unclear. Here, we show that histone H4 is likewise inherited asymmetrically, while histones H2A and H2B are both inherited symmetrically. We hypothesize that the asymmetric distribution of H3 and H4 at sister chromatids is established during DNA replication. To directly visualize histone incorporation pattern on replicating sister chromatids, we develop a chromatin fiber technology with differential labeling of old *versus* new histones. We find spatially separable distributions of old and new H3 on isolated replicating sister chromatids. By contrast, old and new H2A displayed symmetric distribution on replicating sister chromatids. Furthermore, co-localization studies on chromatin fibers and proximity ligation assays on intact nuclei reveal that old H3 are preferentially retained by the leading strand while new H3 preferentially associate with the lagging strand. Finally, using a sequential nucleoside analog incorporation assay, we detect significantly increased unidirectional DNA replication on chromatin fibers from germline compared to somatic cells. Together, the unidirectionality of fork movement coupled with the strandness of histone incorporation could explain the asymmetry between old and new H3 on replicated sister chromatids. In summary, these results indicate that the spatial and temporal asymmetries inherent to DNA replication process may serve to bias histone incorporation, suggesting an unappreciated role for DNA replication in asymmetrically dividing cells.

INTRODUCTION

One of the most fundamental questions in developmental biology is how cells with identical genomes differentiate into distinct cell types. In the process of cell fate specification, epigenetic mechanisms play important roles by altering chromatin structure and gene expression patterns while preserving primary DNA sequences. One important context for understanding cell fate specification is in asymmetric cell division (ACD), where the two daughter cells establish different cell fates following a single division. ACD has been characterized in multiple systems where it plays an essential role in generating cells with distinct fates in development, homeostasis, and tissue regeneration (Betschinger and Knoblich, 2004; Clevers, 2005; Inaba and Yamashita, 2012; Morrison and Kimble, 2006). Stem cells, in particular, often use ACD to give rise to one daughter cell capable of self-renewal and another daughter cell in preparation for terminal differentiation. It is well known that epigenetic mechanisms play a key role in specifying and maintaining stem daughter cell fate, as well as regulating the other daughter cell for proper differentiation pathway (Tarayrah and Chen, 2013; Wu and Sun, 2006; Wutz, 2013). However, it remains unclear how stem cells and differentiating daughter cells might initially establish different epigenomes following ACD, such that the stem cell retains the same epigenetic memory through many divisions while repeatedly producing differentiating daughter cells that carry distinct epigenomes poised for cellular differentiation.

The *Drosophila* male germline stem cell (GSC) system provides a great model to investigate the fundamental molecular and cellular mechanisms underlying ACD (Fuller and Spradling, 2007; Spradling et al., 2011). Previously, using a dual-color strategy to label preexisting (old) *versus* newly synthesized (new) histones, we reported that the old histone H3 is

selectively segregated to the GSC, whereas the new H3 is enriched in the gonialblast (GB) committed for differentiation during ACD of GSCs (Tran et al., 2013; Tran et al., 2012). Subsequently this H3 asymmetry is distinguished through differential phosphorylation at the Thr 3 residue of H3 (H3T3P), followed by specific recognition and segregation during the mitosis of GSCs. Mis-regulation of this key phosphorylation leads to randomized H3 inheritance patterns, as well as severe GSC loss and progenitor germ cell differentiation defects (Xie et al., 2015; Xie et al., 2017). Since post-translational histone modifications are critical components of the epigenome, our studies provide the first direct evidence that stem cells may selectively retain preexisting histones that define its stem cell identity whereas the differentiating daughter cell may reset its epigenome as an initial step in the cellular differentiation program.

In eukaryotic cells, just as DNA must be duplicated *via* replication, chromatin must likewise be established on both strands during and after replication (Alabert and Groth, 2012). Accordingly, the bulk of canonical histones are synthesized and incorporated during DNA replication. Old histones incorporated in nucleosomes on the parental DNA must be disassembled ahead of the replication fork and reassembled onto one of the two new double-stranded DNA (dsDNA) templates behind the fork following DNA synthesis (McKnight and Miller, 1977; Sogo et al., 1986). Although the process of new histone incorporation onto DNA has been well studied, how old histones are recycled during DNA replication is less clear (Burgess and Zhang, 2013). Previous *in vitro* biochemical studies have shown that old histones can display a strand preference toward the leading strand during recycling events in multiple systems (Leffak et al., 1977; Riley and Weintraub, 1979; Roufa and Marchionni, 1982; Seale, 1976; Seidman et al., 1979; Weintraub, 1976). However, many other studies have found no such strand preference and shown that old and new histones have an equal likelihood of association

with either the leading or the lagging strand during replication-coupled nucleosome assembly (Annunziato, 2013, 2015; Cusick et al., 1984; Krude and Knippers, 1991; Sugasawa et al., 1992). Noticeably, the mode of histone incorporation has not been systematically studied in any multicellular organism in the context of cellular differentiation and asymmetric cell division. Characterizing the mechanisms of histone incorporation mode during DNA replication in cells under their physiological condition is critical to our understanding of epigenetic regulation in animal development and various diseases, including cancer and tissue dystrophy [reviewed in (Snedeker et al., 2017)].

RESULTS

Histone H4 Shows Asymmetric Inheritance Pattern during *Drosophila* Male GSC Asymmetric Division

Using a heat shock-controlled switching system to label old histone with GFP (green fluorescent protein) and new histone with mKO (monomeric Kusabira Orange fluorescent protein) (Figures 1A and S1A), we explored the inheritance pattern for all canonical histones following the asymmetric division of male *Drosophila* GSCs. The distributions of old histone (GFP) and new histone (mKO) were measured following the second mitosis after heat shock-induced genetic switch (Tran et al., 2012). Since mitotic GSCs account for less than 2% of the total population of GSCs (Sheng and Matunis, 2011; Tran et al., 2012; Yadlapalli et al., 2011; Yadlapalli and Yamashita, 2013), post-mitotic GSC-GB pairs derived from the asymmetric GSC divisions were first used to visualize and quantify histone inheritance patterns in fixed images (EXPERIMENTAL PROCEDURES). For H4, we found that old H4-GFP was enriched in the GSCs on average 3.3-fold (Figures 1B and 1D), as was previously reported for old H3 (Tran et

al., 2012; Xie et al., 2015). By contrast, such an asymmetric old H4 inheritance pattern was not observed in S-phase spermatogonial (SG) pairs after symmetrical cell division (Figures 1C and 1D). On the other hand, new H4-mKO displayed a more symmetric pattern between GSCs and GBs (Figures 1B and 1D). Presence of newly synthesized H4-mKO in both nuclei of the GSC-GB pair was consistent with the fact that both cells underwent S phase after the second mitosis following heat shock, as indicated by ~ 30-minute nucleoside analog EdU (5-ethynyl-2'-deoxyuridine) incorporation (Figures 1A and 1B). We also examined the H4 segregation pattern in mitotic GSCs. In anaphase (Figure 1E) and telophase (Figure 1F) GSCs, both old H4-GFP and new H4-mKO showed asymmetric segregation patterns. Together, these results establish that histone H4 displayed asymmetric inheritance pattern during ACD, similar to H3.

Histones H2A, H2B and H1 Display Symmetric Inheritance Patterns during *Drosophila* Male GSC Asymmetric Division

Next, we characterized the inheritance patterns of the rest of the canonical histones: H2A and H2B, as well as the linker histone H1 (Figure S1A). Using a similar heat shock-induced switching scheme (Figure 1A), we found that old and new H2A (Figures 2A and 2G) as well as old and new H2B (Figures 2B and 2H) showed symmetric inheritance patterns in post-mitotic GSC-GB pairs. Further investigation of mitotic GSCs at anaphase confirmed this globally symmetric inheritance pattern for both H2A (Figure 2C) and H2B (Figure 2D). Additionally, both H2A (Figures 2E and 2G) and H2B (Figures 2F and 2H) displayed symmetric old and new histone inheritance patterns in post-mitotic SG pairs. Finally, the linker histone H1 also showed globally symmetric inheritance pattern in post-mitotic GSC-GB pairs (Figure S1B).

Overall, histones H3 and H4 showed significantly greater asymmetric distributions in asymmetrically dividing GSCs when compared to H2A and H2B. These findings indicate that even though H3, H4, H2A, H2B, and H1 are all initially incorporated in a replication-dependent manner, different histones display distinct inheritance patterns in *Drosophila* male GSCs. This can be explained by incorporation dynamics at the replication fork, or different stabilities and/or exchange rates post-replication. To our current knowledge, H3 and H4 have the majority of known post-translational modifications and may act as the major epigenetic information carriers (Allis and Jenuwein, 2016; Kouzarides, 2007; Young et al., 2010). Our previous studies have also shown that the histone variant H3.3 does not exhibit asymmetric inheritance pattern during ACD of GSCs (Tran et al., 2012). Because H3 and H4 are incorporated during DNA replication whereas H3.3 can be incorporated in a replication-independent manner, we hypothesize that the establishment of the H3 and H4 asymmetries occurs during DNA replication, when old H3 and H4 are retained by one set of sister chromatids, while new H3 and H4 are differentially incorporated into the other set of sister chromatids.

Establishing the Chromatin Fiber Technique to Directly Visualize Sister Chromatids

In order to directly examine histone incorporation patterns on newly replicated DNA, we adapted the chromatin fiber technique (Ahmad and Henikoff, 2002; Blower et al., 2002; Cohen et al., 2009) to extract EdU pulse-labeled DNA with associated proteins, including histones for direct visualization. To validate this technology, we first examined chromatin fibers isolated from *Drosophila* embryos at the syncytial blastoderm stage and compared them with previous electron microscopy images of chromatin fibers from the similar staged embryos (McKnight and Miller, 1977). Indeed, unreplicated (Figures 3A and 3B, 3D and 3E) and newly replicated (Figures 3A

and 3C, 3D and 3F) regions could be clearly distinguished using a short pulse of EdU (EXPERIMENTAL PROCEDURES). In addition, at the EdU-positive regions, broader fiber structure and brighter DNA staining with DAPI (Figures 3A and 3D) or YOYO (Figure 3G) DNA dye could be detected compared to EdU-negative regions, as reported previously (Cohen et al., 2009). The EdU-positive replicating regions ranged from 250nm to 8μm long, which are comparable with previous reports using electron microscopy (Blumenthal et al., 1974; McKnight and Miller, 1977; Wolstenholme, 1973). Approximately 3.2% (*n*=250) replication regions showed wide separation between the two sister chromatids as far as 500nm-800nm apart, which could be visualized as double fibers using confocal microscopy (Figures 3D and 3F).

To overcome resolution limits of confocal microscopy, two high resolution microscopy methods were used to resolve sister chromatids at replicating regions along chromatin fibers: Stimulated Emission-Depletion (STED) microscopy and Zeiss Airyscan imaging method. Using STED microscopy, we were able to resolve the DAPI/YOYO bright regions into two sister chromatid fibers (Figures 3G and 3I). Similar structures could be visualized using Airyscan imaging, despite at a lower frequency (Figure 3J). This is likely due to the lower resolution of Airyscan (~150 nm) (Ke et al., 2016) compared to STED (~35 nm) (Hell and Wichmann, 1994). Overall, the percentage of spatially resolvable sister chromatids from EdU-positive chromatin fibers isolated from testes ranged from 0.8% using confocal to 8.6% using Airyscan, to 25% using STED (Figure 3J). Since these resolvable percentages from the same samples are proportional to the spatial resolution using different microscopy methods, we conclude that high resolution microscopy methods, such as Airyscan and STED, greatly facilitate recognition of sister chromatids at replicating or newly replicated chromatin fibers. The application of superresolution microscopy on replicating chromatin fibers represents a new methodology to

study DNA replication and nucleosome assembly, which can be used in a wide variety of contexts.

Noticeably, even though some EdU-positive region could be resolved into double sister chromatids (upper EdU-positive region in Figure S2A), not all EdU-positive region could be unambiguously resolved into double fibers (lower EdU-positive region in Figure S2A). These STED unsolvable replicating and/or replicated fibers likely represent regions where the two sister chromatids are tightly cohesed and are technically difficult to be resolved. Indeed, RAD-21, a key component of the cohesin complex, which has been shown to associate with chromatin during and after passage of the replication fork (Tittel-Elmer et al., 2012; Zheng et al., 2018), showed enrichment at the replication bubble in between the two newly replicated sister chromatids (Figures 3K and 3L). In spite of these limitations, a great number of replicating chromatin fibers can be resolved into sister chromatids using superresolution microscopy techniques, allowing us to apply them in our studies.

Distinct Patterns between Old H3 *versus* new H3 and Old H2A *versus* New H2A on Sister Chromatids

Using this chromatin fiber technique with high resolution microscopy methods, we next explored old and new histone distribution on chromatin fibers isolated from the early-stage *Drosophila* male germ cells (EXPERIMENTAL PROCEDURES). A similar genetic switch was applied to label old H2A or H3 with eGFP and new H2A or H3 with mCherry (Figure S1A). Using Airyscan imaging, unreplicated regions were detected as a single fiber structure enriched with either old H2A-eGFP only (Figures 4A and 4B) or old H3-eGFP only (Figures 4F and 4G), but devoid of new histones and EdU. Similar results were obtained for old H3-GFP using STED

(Figure 4J). In comparison, chromatin fiber regions where sister chromatids could be resolved correlated with EdU signals and showed enrichment for new histones H2A (Figures 4A and 4C) and H3 (Figures 4F and 4H). Co-localization between EdU-positive region and new histones further confirmed that these double fiber structures are replicating or newly replicated chromatin regions.

Examination of old H2A-eGFP *versus* new H2A-mCherry revealed overall symmetric distribution between the two sides of the replication bubble representing newly replicated sister chromatids (Figures 4A and 4C). By contrast, old H3-eGFP and new H3-mCherry displayed asymmetric patterns on newly replicated sister chromatid fibers (Figures 4F and 4H). Consistently, two-color STED imaging showed similar asymmetric old H3-GFP and new H3-mKO distribution between sister chromatids (Figures 4I and 4K).

In order to systematically compare histone distribution patterns between H3 and H2A along sister chromatids, we divided double chromatin fibers into 2μm segments and measured the fluorescence levels for both old and new histones on each sister chromatid (Figure S3, EXPERIMENTAL PROCEDURES). By assessing histone enrichment on sister chromatin fibers, old H3 showed on average a 2.41±0.20-fold difference between the two sides (Figure 4D), with 44.3% of fiber segments (n=61) showing greater than 1.80-fold difference. By comparison, old H2A showed a 1.36±0.04 ratio between sister chromatids (Figure 4D), with only 10.9% fiber segments (n=64) showing greater than 1.80-fold difference. We used the 1.80-fold as a criterion, based on one-standard deviation above the average ratio of old H2A fiber segments to define the symmetric range, which represents a stringent cut-off for calling ‘asymmetry’ between sister chromatids. Overall, old H3 displayed significantly higher incidence of asymmetry than did H2A fibers (Figure 4D, $P < 10^{-4}$).

On the other hand, new H3 showed on average a 1.94±0.16-fold difference between the two sides of double chromatin fibers (Figure 4E), with 39.0% of fiber segments (n=59) showing greater than 1.70-fold difference. By comparison, new H2A showed a 1.24±0.06 ratio between sister chromatids, with only 11.1% fiber segments (n=45) showing greater than 1.70-fold difference (Figure 4E). Similarly, here the 1.70-fold was used as a cutoff based on one-standard deviation above the average ratio of new H2A fiber segments. Overall, distribution of new H3 on sister fibers also showed a significantly higher incidence of asymmetry than new H2A fibers (Figure 4E, $P < 10^{-3}$). In summary, these results suggest that both old and new H3 are more differentially incorporated during DNA replication compared to old and new H2A. These patterns are consistent with the different segregation patterns between H3 and H2A in mitotic GSCs, suggesting that differential histone incorporation during S phase could underlie asymmetric H3 but symmetric H2A inheritance patterns.

Differential Incorporation of Old and New H3 Correlate with Strand-enriched DNA Replication Components

As H3 show significant asymmetries during the process of replication-coupled nucleosome assembly, we next tested whether old *versus* new H3 asymmetry correlates in any way with strand-enriched DNA replication machinery components. To test the strand specificity of old and new histones, we imaged old H3-GFP and new H3-mKO on isolated chromatin fibers immunostained for proliferating cell nuclear antigen (PCNA), a key replication component enriched at the lagging strand (Yu et al., 2014). Consistent with the role of PCNA in replication, PCNA signals colocalized with new H3 along the chromatin fiber (Figure S4). At the regions where sister chromatids could be resolved, the PCNA signal was enriched on sister chromatid

with new H3-mKO whereas old H3-GFP was relatively depleted on the PCNA-enriched side (Figures 5A and 5B). Overall, old H3-GFP showed a significantly greater level of enrichment at the PCNA-depleted sister chromatid (leading strand, $P<10^{-4}$), whereas new H3-mKO showed a significantly higher level of enrichment at the PCNA-enriched sister chromatid (lagging strand, $P<10^{-4}$, Figure 5C), suggesting that old histones are likely selectively recycled to the leading strand while new histones are incorporated to the lagging strand.

To further explore the strand preference of H3 incorporation during DNA replication, we isolated chromatin fibers with eGFP-tagged Replication protein A (RPA) in its endogenous genomic context (*rpa>RPA-eGFP)* (Blythe and Wieschaus, 2015). Similar to PCNA, RPA is a highly conserved single-stranded DNA-binding protein, which is significantly enriched at the lagging strand (Wold, 1997). As RPA is tagged with eGFP, we were unable to image RPA together with the two-color histone labeling system using eGFP or GFP. Therefore, we utilized the H3K27me3 histone modification, which has been previously shown to be highly enriched with old histones during S phase (Alabert et al., 2015a; Lin et al., 2016). Indeed, at the EdU-positive sister chromatid regions, RPA and H3K27me3 occupied the opposite sister chromatids (Figures 5D and 5E), further suggesting that old H3 is recycled to the leading strand. Quantification of the RPA-labeled chromatin fibers showed an average of 11.0-fold difference of the H3K27me3 distribution at the RPA-depleted fiber compared to the RPA-enriched fiber (Figure 5F, $P< 10^{-4}$). Noticeably, this asymmetry for H3K27me3 is greater than that for old H3 labeled with GFP using the dual-color transgene (Figure 4D). We reason that the fact H3K27me3 is mostly, if not entirely, carried by old H3 at the replication fork, whereas H3-GFP stands for the transgenic but not the endogenous H3. Another potential reason is that using the heat shock-induced genetic switch, the representation of H3-GFP as a proxy for old H3 depends on the

timing of the switch in the context of cell cycle. For example, if the switch occurs in the mid-S phase, some of the H3-GFP has already been used as new histones. Taken together, these results indicate that during DNA replication, old H3 is preferentially recycled by the leading strand whereas new H3 is incorporated onto the lagging strand.

Proximity Ligation Assay Reveals Strand Preference between Old and New H3 during Replication-coupled Nucleosome Assembly

While the chromatin fiber technique offers many advantages by directly visualizing the distribution of old and new histones on sister chromatids, the process of lysing the nuclei makes it extremely difficult to retain information related to the germline stage specificity. To further explore histone inheritance pattern at the replication fork in a stage-specific manner, we used an imaging based proximity ligation assay (PLA) to probe the spatial proximity between histones (old *versus* new) and different strand-enriched DNA replication components. The PLA method enables positive fluorescence detection if two proteins of interest are in close proximity (< 40 nm), which has been previously used in *Drosophila* embryos to address protein-protein proximity at the replication fork (Petruk et al., 2012). To verify that PLA using antibodies against DNA replication components show signals specific to S-phase cells, PLA puncta in non-replicating somatic hub cells were quantified and showed almost no signal (Figure S5A). Furthermore, to confirm PLA using antibodies against DNA replication components show signals specifically with nuclear proteins, control PLA experiments were performed between histones and a cytoplasmic protein Vasa (Lasko and Ashburner, 1990), which also showed extremely low PLA signal (Figure S5A). Results from these control experiments confirmed that PLA signals are specific in replicating nuclei and the false positive signal is minimal.

To investigate the strandness of old *versus* new histones, we used CRISPR/Cas9-mediated genome editing (Horvath and Barrangou, 2010; Wright et al., 2016) to tag the lagging strand-enriched DNA ligase at its endogenous genomic locus using a 3xHA epitope. We then applied anti-HA for the PLA assay to probe the spatial proximity between histones (old *versus* new) and ligase, which serves as a proxy for the lagging strand. We observed a higher number of PLA fluorescent puncta between ligase and new H3-mKO (Figure 6A) than those between ligase and old H3-GFP (Figure 6B). Quantification of the overall PLA signals in GSCs showed significantly more PLA fluorescent puncta between ligase and new H3 than those between ligase and old H3 (Figure 6C, $P < 0.01$).

Next, we used another lagging strand-enriched component, PCNA, as a marker for the PLA experiments. We also observed a higher number of PLA fluorescent puncta between PCNA and new H3-mKO (Figure 6D) than those between PCNA and old H3-GFP (Figure 6E). Again, quantification of the overall PLA signals showed significant more PLA fluorescent puncta between PCNA and new H3-mKO than those between PCNA and old H3-GFP in GSCs (Figure 6F, $P < 0.001$). As a control, we also performed PLA experiments using a strain where the tags for old H3 and new H3 were swapped with old H3-mKO and new H3-GFP. Consistent with the previous results, more PLA fluorescent puntae were obtained between PCNA and new H3-GFP (Figure S5B) than the signals between PCNA and old H3-mKO (Figure S5C). Quantification of these control experiments showed significant more PLA signals with new H3 (Figure S5D, $P < 0.05$), regardless of the identity of the tags, suggesting that the PLA results reflect the molecular differences between old and new H3. Together, these results are consistent with the chromatin fiber experiments shown in Figure 5, suggesting that new H3 preferentially associates with the lagging strand.

Unlike GSCs, SGs showed no significant strand preference between old and new histones for either ligase (Figure 6C) or PCNA (Figure 6F). This suggests that the asymmetry observed at the replication fork during DNA replication becomes less pronounced as germ cells differentiate, consistent with previous results (Tran et al., 2012) (Figure 1). These findings further demonstrate that histone distribution patterns show a cellular specificity not only during mitosis, but also during DNA replication.

Nucleoside Analog Incorporation Assay Reveals High Incidence of Unidirectional Fork Progression in *Drosophila* Male Germline

Up to now, we have demonstrated that during DNA replication, old H3 are reincorporated by the leading strand whereas new H3 are preferentially incorporated on the lagging strand. However, if replication forks are proceeding outward from replication origins in a bidirectional manner, asymmetries in histone inheritance at the replication fork alone would lead to alternating stretches of leading-strand-incorporated old histones and lagging-strand-incorporated new histones on each of the two duplicating sister chromatids (Figure 7A), which would not be sufficient to explain the global asymmetry of histone inheritance we have observed. Therefore, we hypothesize that mechanisms exist to coordinate replication forks, in order to achieve long-range histone asymmetric patterns.

To explore whether fork movement might be coordinated in the *Drosophila* germline, we turned to the chromatin fiber method and utilized a sequential nucleoside analog incorporation assay: active DNA replication regions were first labeled with EdU and subsequently by BrdU (EXPERIMENTAL PROCEDURES). By using sequential pulses of EdU and BrdU to assess fork movement, the progression of replication forks in bidirectional manner (Figure 7C) and

unidirectional manner (Figure 7D) would be expected to produce distinct patterns. We found that chromatin fibers derived from somatic cells, such as larval imaginal disk cells, displayed largely bidirectional fork movement (Figure 7E). Quantification of these data demonstrated that 87% of replicons identified on chromatin fibers from somatic cells (*n*=31) showed EdU signal flanked by BrdU signals on both sides (Figures 7E and 7G); a pattern typical for bidirectional fork movement. In contrast, a substantial fraction (43.0%) of germline-derived chromatin fibers (*n*=31) contained replicons with unidirectional replication progression, for which EdU signal was adjacent but not flanked by the BrdU signal (Figures 7F and 7G). Furthermore, fork movement in unidirectional replicons appeared to be coordinated, as multiple unidirectional forks appeared to move toward the same direction (Figure 7F).

To further explore replication patterns in the *Drosophila* male germline, we utilized an alternative strategy to track fork progression using the relative positions between new histones (H2A-mCherry) and EdU introduced by a short pulse on chromatin fibers. New H2A marks both actively replicating and post-replicative regions, while a short EdU pulse just prior to fiber preparation only labels the most recently replicated and replicating region. Using this assay, a bidirectional fork movement would lead to EdU signals flanking the stretch of new histone incorporated region on both sides (Figure 7H). By contrast, a unidirectional fork movement would result in EdU signal localized to only one side of the new histone region (Figure 7I). Indeed, distinguishing and quantifying these two patterns using male germline-derived chromatin fibers showed 48% (*n*=33) unidirectional fork movement (Figures 7K and 7L) and 52% (*n*=33) bidirectional fork movement (Figures 7J and 7L). Overall, the percentage of unidirectional fork movement using both methods gave out very similar results (43% *versus* 48%). Taken together, these results reveal that replication could be coordinated in the *Drosophila* germline to allow for

unidirectional fork movement (Figure 7B). Together with the detected strand bias found between old and new histones, these mechanisms would expand asymmetric histone incorporation at individual forks to global asymmetries between sister chromatids.

DISCUSSION

In this work, we utilized a series of imaging-based approaches to explore whether and how DNA replication contributes to asymmetric histone inheritance in *Drosophila* male GSCs. Our data demonstrate that preexisting H3 preferentially associate with the leading strand while newly synthesized H3 are incorporated into the lagging strand during DNA replication. Additionally, our data suggest that in the *Drosophila* germline, replication fork progression is highly coordinated, linking the asymmetry at the replication fork to the previously reported histone asymmetry between sister chromatids during mitosis. As such, DNA replication may play a novel, unappreciated role in directing histone incorporation on two identical, replicating DNA strands, and may differentially establish epigenetic information on two sister chromatids.

This study has adapted several technical innovations. First, we have optimized the chromatin fiber technique and combined it with different high spatial resolution microscopy methods to visualize sister chromatids as they are undergoing the processes of DNA replication and replication-coupled nucleosome assembly. Combining this technique with the dual-color histone labeling system and/or immunostaining for histone modifications, we established a novel method to study replication-coupled nucleosome assembly at sister chromatids. Noticeably, this information would be very difficult to attain by other means. For example, any sequencing-based method would not be able to distinguish sister chromatids because they are genetically identical. Therefore, our findings will have important implications for understanding epigenetic

inheritance, specifically the process of replication-coupled nucleosome assembly. Prior work has demonstrated that nucleosomes which are displaced ahead of the replication fork are recycled almost immediately with extremely high efficiency (Alabert et al., 2015b; Verreault, 2003; Worcel et al., 1978). Due to the continuous nature of leading strand synthesis, it has been hypothesized that old histones may preferentially associate with the leading strand during the process of histone recycling (Annunziato, 2013; Seidman et al., 1979). Accordingly, EM studies of replicating SV40 viral chromosomes have demonstrated that histones tend to associate with the leading strand sooner (~225nt after fork passage) than with the lagging strand (~285nt after fork passage) (Sogo et al., 1986). While large-scale asymmetries in the deposition of histone proteins have been observed experimentally (Riley and Weintraub, 1979; Seale, 1976; Seidman et al., 1979; Sogo et al., 1986; Weintraub, 1976), a majority of studies have demonstrated that on a global scale, old and new histones are equally associate with the leading and lagging strands following replication (Alabert and Groth, 2012; Annunziato, 2013; Jackson and Chalkley, 1981a, 1985). These findings suggest that the fundamental differences between leading strand and lagging strand replication may not be sufficient to bias histone inheritance patterns globally across many cell types. However, this question had not been addressed thoroughly in a multicellular organism in a developmental context. Here we have been able to study old and new histone distribution patterns at sister chromatid resolution. Our results suggest that histone incorporation patterns have molecular specificity. On newly replicated sister chromatids, old and new H3 show a significantly higher incidence of asymmetry between sister chromatids than do old and new H2A. These findings suggest that different histones may behave differently during the process of chromatin recycling and maturation. Previous biochemical studies have established that H3 and H4 are incorporated as a tetramer $(H3\text{-}H4)_2$, while H2A and H2B are

incorporated as dimers (Annunziato et al., 1982; Jackson, 1988; Jackson and Chalkley, 1981a, b; Katan-Khaykovich and Struhl, 2011; Russev and Hancock, 1981; Xu et al., 2010). Moreover, H2A and H2B exhibit much more dynamic behavior compared to $(H3\text{-}H4)_2$ tetramers (Kimura, 2005). For H2A and H2B, which split into two separate dimers, it is conceivable that old-H2A (or H2B) dimers may be more easily inherited symmetrically on newly replicated sister chromatids. In contrast, $(H3\text{-}H4)_2$ tetramers rarely split (Xu et al., 2010), meaning that mixed nucleosomes containing both old and new (H3-H4) dimers hardly ever form. Indeed, the similar asymmetric inheritance pattern of old H3 and H4 suggested that the preexisting $(H3\text{-}H4)_2$ tetramers were inherited as a whole unit, consistent with the previous report (Xu et al., 2010).

On the other hand, the range of old and new H3 distribution between sister chromatids (Figures 4D and 4E) suggests that the process of replication-coupled nucleosome assembly may not be uniformly regulated throughout the genome and in all cell types. Rather, factors such as cell type- and stage-specificity, as well as genomic context may play important roles in regulating the distribution of old and new histones at the replication fork. Indeed, results from our PLA studies suggest that the process of histone recycling may be subject to regulation in a cell-type specific manner, as asymmetrically dividing GSCs showed a more pronounced asymmetry at the fork than did symmetrically dividing SGs (Figures 6C and 6F).

Using different regimes of the thymidine analogue incorporation, directionality of replication fork movement could be precisely visualized (Figures 7D-G and 7I-L). Studies in replication fork progression have demonstrated that in most contexts, two replication forks progress outward at similar rates from a single origin of replication to create a bidirectional pattern of replication fork progression (Abdurashidova et al., 2000; Burhans et al., 1990; Cairns, 1963, 1966; Huberman and Riggs, 1968; Li and Kelly, 1985; Merrick et al., 2004; Nieminuszczy

et al., 2016). Studies on mammalian replicons have identified that approximately 5% of origins are replicated in a unidirectional manner whereas 95% are bidirectional (Hand, 1975). Consistent with low incidence of unidirectional fork movement, in our studies using *Drosophila* somatic cells, 13% of replicons showed unidirectional fork movement while 87% were bidirectional. In contrast, replication fork progression in the *Drosophila* germline showed a significantly higher incidence of unidirectional replication (43.0% using sequential nucleoside analog incorporation and 48.0% using short pulse analog with new H2A pattern). Noticeably, the percentages of chromatin fibers showing substantial H3 asymmetries (44.3% for old H3 and 39.0% for new H3) are comparable with the percentage of fibers showing unidirectional fork movement (43.0% using sequential nucleoside analog incorporation and 48.0% using short pulse analog with new H2A pattern), suggesting a potential connection between these two phenomena. Unidirectional replication and coordinated fork movement are by no means unprecedented observations (Martin-Parras et al., 1991). Fork block systems in the replicating *S. pombe* are utilized during mating-type switching to help coordinate fork movement across the mating type locus to create a DNA lesion necessary for initiating the DNA repair mechanisms involved in the process of mating-type switching (Dalgaard and Klar, 2001). In *Drosophila*, it has been shown that fork movement at the rDNA region is unidirectional (Sasaki et al., 1999). Fork block systems have also been found in metazoan systems to ensure that replication/transcription collisions do not occur in the context of the heavily transcribed loci (Buck et al., 2002). However, fork coordination across broad stretches of the genome as a means to regulate epigenetic inheritance represent a previously uncharacterized aspect of cell-type specific regulation of DNA replication.

Finally, it has long been recognized that DNA replication is an inherently asymmetric process. Both the molecular components and temporal order of the synthesis of the leading and

lagging strands are distinct. Previous work has demonstrated that many cells overcome this asymmetry by regulating the progression of the replication fork, such that both strands are synthesized concurrently with replication fork progression, leading to simultaneous synthesis of two genetically identical sister chromatids (Alberts et al., 1983; Bermek et al., 2015; Debyser et al., 1994; Hamdan et al., 2009; Lee et al., 1998; Lee et al., 2006; Prelich and Stillman, 1988; Stano et al., 2005; Stengel and Kuchta, 2011; Yao et al., 2009). However, studies perturbing key molecular players involved in DNA replication have shown that it is possible to uncouple these two processes (Kadyrov and Drake, 2002; Yang et al., 2006; Yeeles and Marians, 2013). Furthermore, recent single molecule *in vitro* studies have suggested an alternative model, in which each polymerase proceeds in a stochastic manner, such that long gaps (kilobases in length) in sister chromatid synthesis could occur as a result of temporal and spatial separation between leading strand and lagging strand synthesis (Graham et al., 2017). Here, our results demonstrate that old H3 more readily associate with the leading strand whereas new H3 more frequently associate with the lagging strand. Previous studies suggest that the leading strand is synthesized continuously, which may serve as a more suitable substrate for nucleosome binding than the discontinuously synthesized lagging stand. This is due to the fact many factors associated with lagging strand synthesis, such as RNA-DNA hybrids, ssDNA and DNA bound by RPA and PCNA have been shown to be less favorable substrates for nucleosome incorporation compared to dsDNA (Almouzni et al., 1990; Dunn and Griffith, 1980; Janke et al., 2018). As old histone recycling occurs in a nearly instantaneous fashion (Huang et al., 2015), it is conceivable that transient delays in lagging-strand synthesis could bias old histone recycling and result in the asymmetric pattern. Indeed our RPA studies demonstrate that old histone (marked by

H3K27me3) are largely absent in newly replicated areas where RPA is still bound at those regions not been fully synthesized (Figure 5D).

In summary, our work demonstrates that the intrinsic asymmetries in DNA replication process may help construct sister chromatids enriched with distinct populations of histones. These findings suggest at the exciting possibility that DNA replication can be exploited in a cell-type specific manner. While the molecular players responsible for this cell-type-specificity remain unclear, this demonstration of a potential regulatory role for DNA replication represents an important step forward in understanding how DNA replication and replication-coupled nucleosome assembly intersect to regulate distinct epigenetic identities of different cell types.

Figures and Figure Legends:

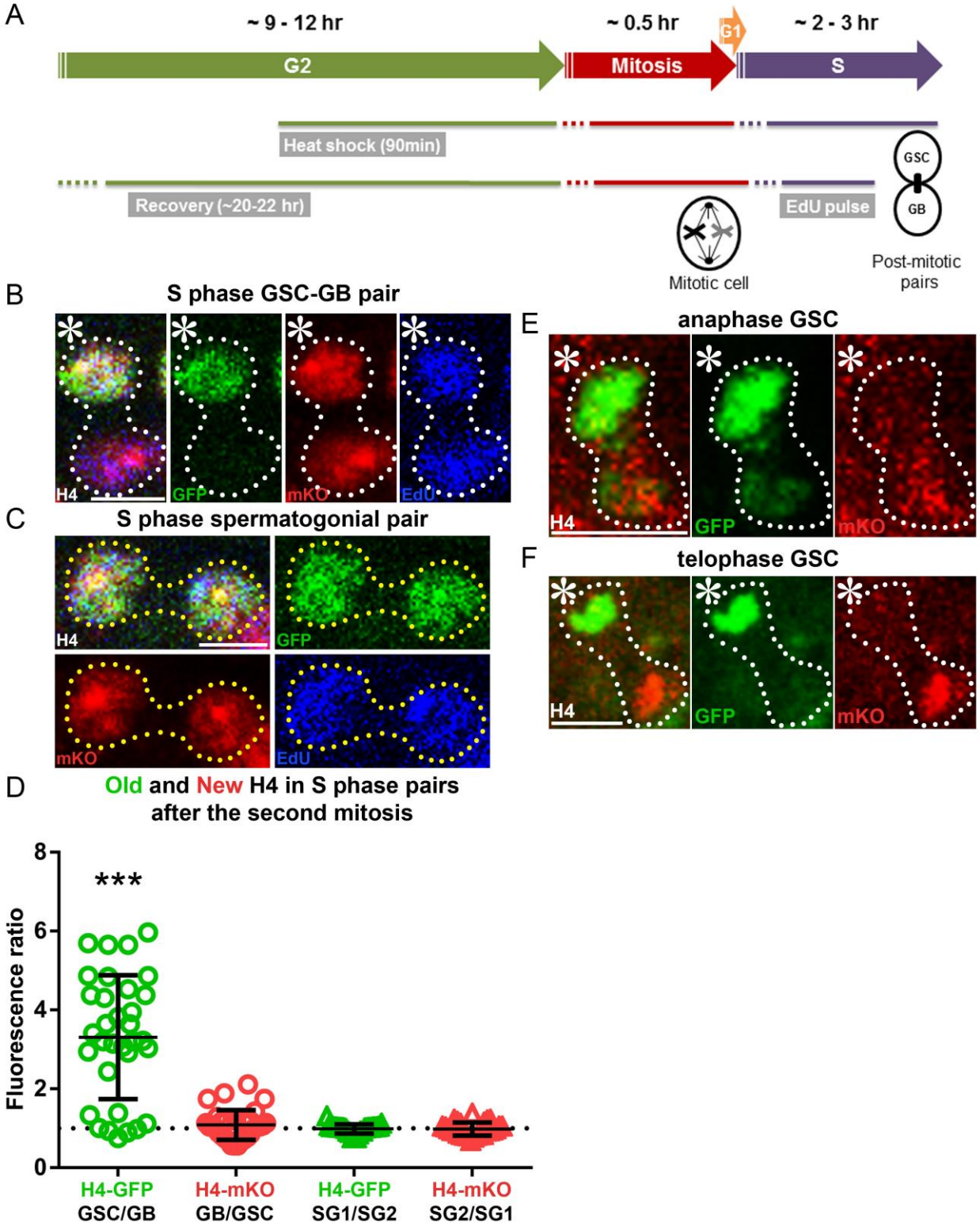

Figure 1: Histone H4 shows asymmetric inheritance pattern during *Drosophila* GSC asymmetric divisions. (**A**) A cartoon depicting the experimental design. (**B**) H4 distribution patterns in a post-mitotic GSC-GB pair labeled with EdU (blue): H4-GFP (green) is distributed asymmetrically towards the GSC whereas H4-mKO (red) distributed more evenly between the GSC and the GB. (**C**) H4 distribution patterns in a post-mitotic SG pairs. Both H4-GFP and H4-mKO are symmetrically distributed between the two SG nuclei. (**D**) Quantification of both H4-GFP and H4-mKO distributions in GSC-GB pairs (n=33) and SG1-SG2 pairs (n=27). See Table S1 for details. (**E**) An anaphase GSC showing asymmetric segregation of H4-GFP towards the GSC and H4-mKO towards the GB. (**F**) A telophase GSC showing asymmetric distribution of H4-GFP towards the GSC and H4-mKO towards the GB. *** $P < 0.0001$, two-tailed student's t-test if average significantly different than 1. Scale bar: 5μm. Asterisk: hub.

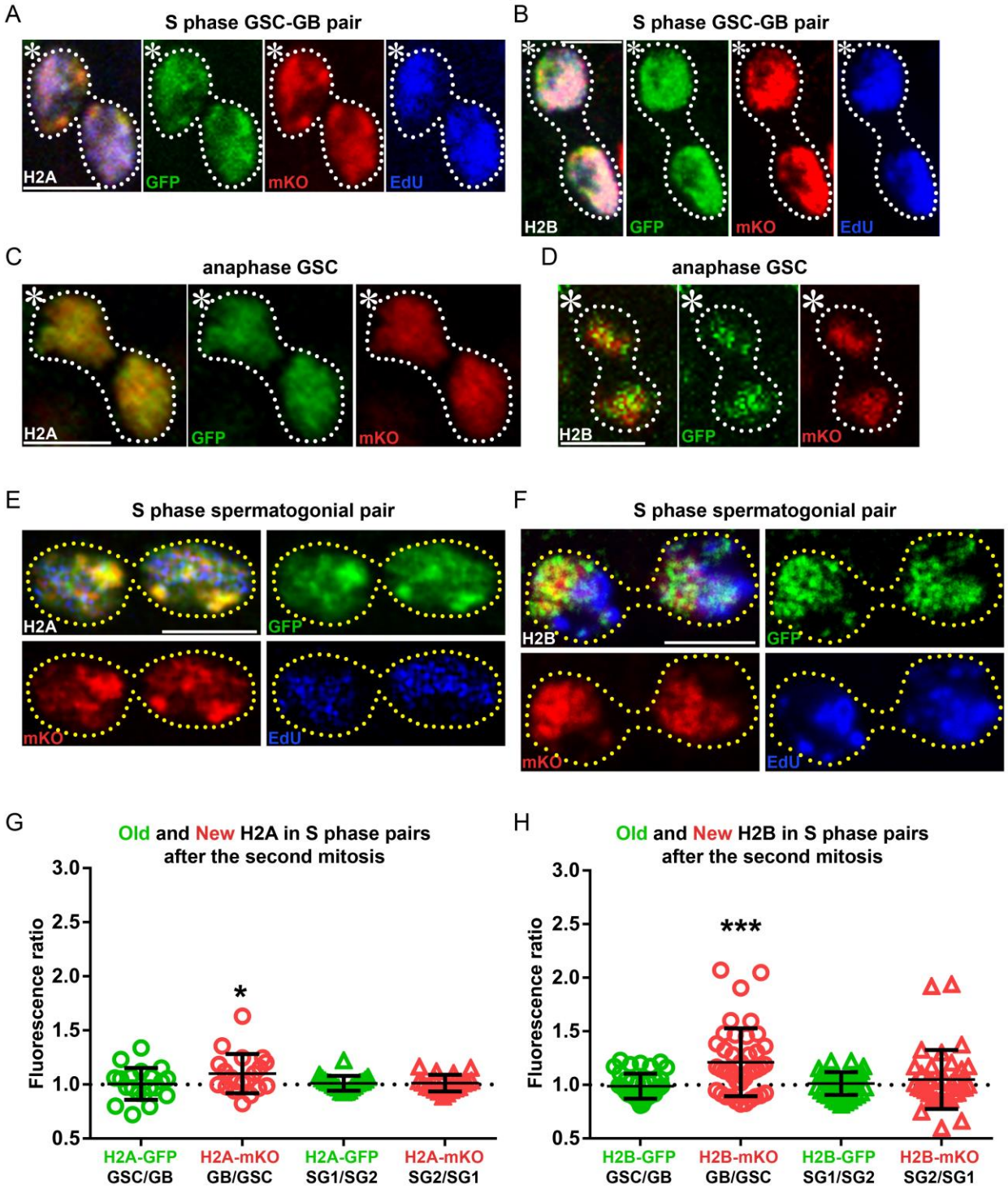

Figure 2: Histones H2A and H2B show symmetric distribution during *Drosophila* GSC asymmetric division. (**A**) Symmetric H2A inheritance pattern in a post-mitotic GSC-GB pair. **(B)** Symmetric H2B inheritance pattern in a post-mitotic GSC-GB pair. (**C**) An anaphase GSC

showing symmetric segregation of H2A-GFP and H2A-mKO. (**D**) An anaphase GSC showing symmetric segregation of H2B-GFP and H2B-mKO. (**E**) Symmetric H2A inheritance pattern in a post-mitotic SG pair. (**F**) Symmetric H2B inheritance pattern in a post-mitotic SG pair. (**G**) Quantification of H2A-GFP and H2A-mKO distribution in GSC-GB pairs (n= 20) and SG1-SG2 pairs (n= 20). See Table S2 for details. (**H**) Quantification of H2B-GFP and H2B-mKO distribution in GSC-GB pairs (n= 40) and SG1-SG2 pairs (n= 36). See Table S3 for details. *** P< 0.0001, * P< 0.05, two-tailed student's t-test if average significantly different than 1. Both new H2A and new H2B show a subtle, but statistically significant enrichment in GB compared to GSC in post-mitotic pairs, likely due to asynchronous ongoing S phase in both GB and GSC nuclei. Scale bar: 5μm. Asterisk: hub.

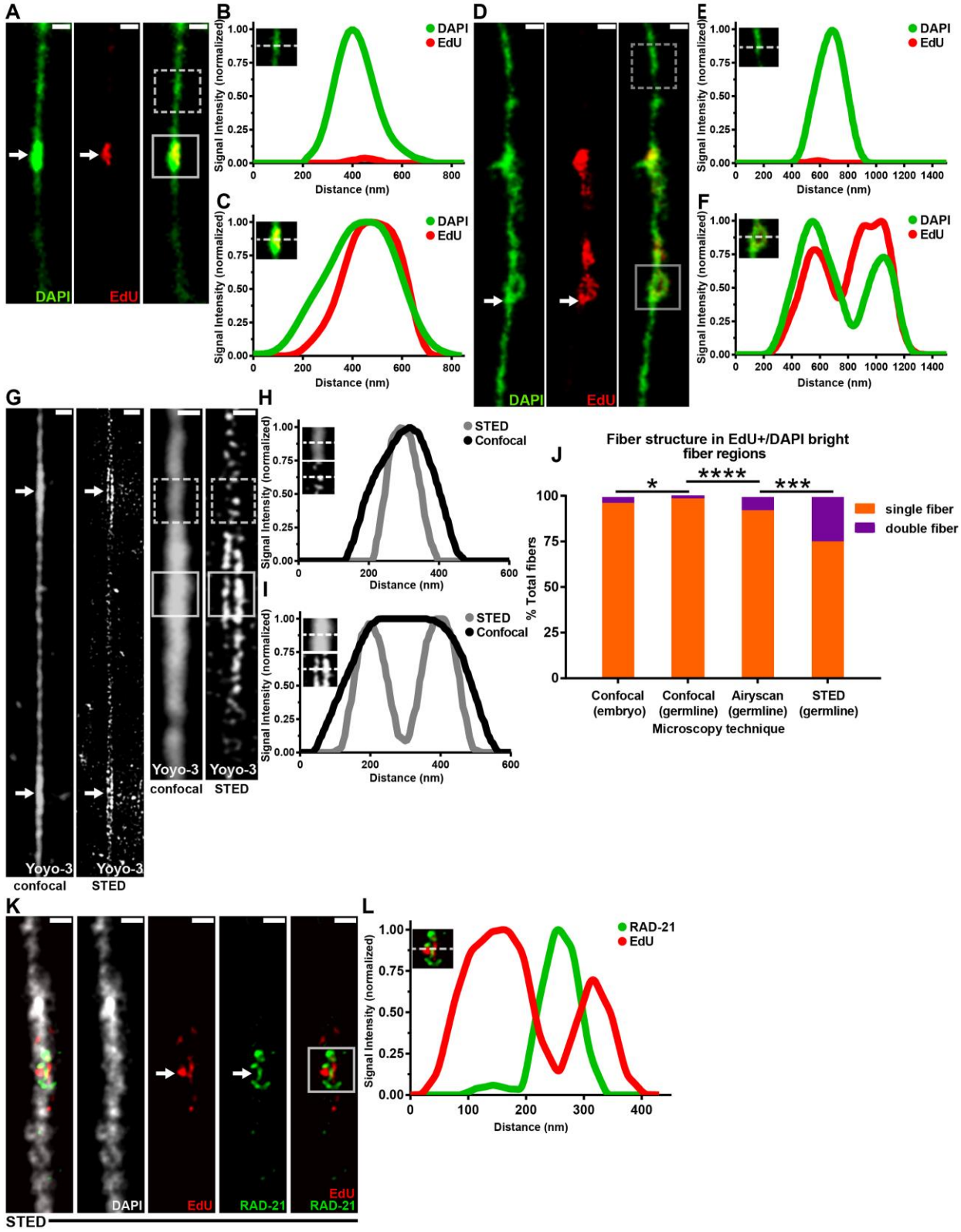
A
DAPI
EdU
B
DAPI
EdU
Signal Intensity (normalized)
Distance (nm)
C
DAPI
EdU
Signal Intensity (normalized)
Distance (nm)
D
DAPI
EdU
E
DAPI
EdU
Signal Intensity (normalized)
Distance (nm)
F
DAPI
EdU
Signal Intensity (normalized)
Distance (nm)
G
Yoyo-3
Yoyo-3
confocal
STED
Yoyo-3
Yoyo-3
confocal
STED
H
STED
Confocal
Signal Intensity (normalized)
Distance (nm)
I
STED
Confocal
Signal Intensity (normalized)
Distance (nm)
J
Fiber structure in EdU+/DAPI bright fiber regions
*
****
***
single fiber
double fiber
% Total fibers
Confocal (embryo)
Confocal (germline)
Airyscan (germline)
STED (germline)
Microscopy technique
K
DAPI
EdU
RAD-21
EdU
RAD-21
STED
L
RAD-21
EdU
Signal Intensity (normalized)
Distance (nm)

Figure 3: Superresolution microscopy helps visualize sister chromatids on isolated chromatin fibers. (**A**) Confocal image of chromatin fiber isolated from *Drosophila* embryos showing replication "bubble" structure with EdU and brighter DAPI signal (white arrow). Scale bar: 500nm. (**B**) Line-plot shows DAPI and EdU distribution on unreplicated region without EdU (box with dotted white lines in **A**, inset in **B**). (**C**) Line-plot shows DAPI and EdU distribution on replicated region with EdU (box with solid white lines in **A**, inset in **C**). Replicated region appears thicker [400nm full-width half maximum (FWHM)] than un-replicated region (250nm FWHM). However, sister chromatids cannot be clearly resolved. (**D**) Confocal image of chromatin fiber isolated from *Drosophila* embryos contains replicating bubble structure with DAPI showing transition from single fiber to double fiber structure at the point where EdU incorporation becomes apparent (white arrow). Scale bar: 500nm. (**E**) Line-plot shows DAPI and EdU distribution on unreplicated region without EdU (box with dotted white lines in **D**, inset in **E**). (**F**) Line plot shows DAPI and EdU distribution on replicated region with EdU (box with solid white lines in **D**, inset in **F**). (**G**) Confocal and STED images of chromatin fiber isolated from *Drosophila* male germline, stained with DNA dye Yoyo3. Yoyo bright regions (white arrows) can be resolved into sister chromatids with STED. Scale bar: 500nm. (**H**) Line plot on Yoyo3 dim region shows a single fiber structure with both confocal and STED (box with dotted white lines in **G**, inset in **H**). (**I**) Line-plot in replicating/replicated (Yoyo3 bright) region shows clear double fiber structure with STED but not with confocal (box with solid white lines in **G**, inset in **I**). (**J**) Quantification of the frequency seeing single *versus* double fiber structure at EdU-positive and DAPI-bright regions. **** $P < 0.0001$, *** $P < 0.001$,* $P < 0.05$, Chi-squared test. (**K**) STED image of chromatin fiber extracted from *Drosophila* male germline labelled with EdU and immunostained for RAD-21, a cohesin component at the replication bubble (white arrow).

Scale bar: 500nm. (**L**) Line-plot shows RAD21 signal in between two EdU-positive sister chromatids (box with solid white lines in **K**, inset in **L**).

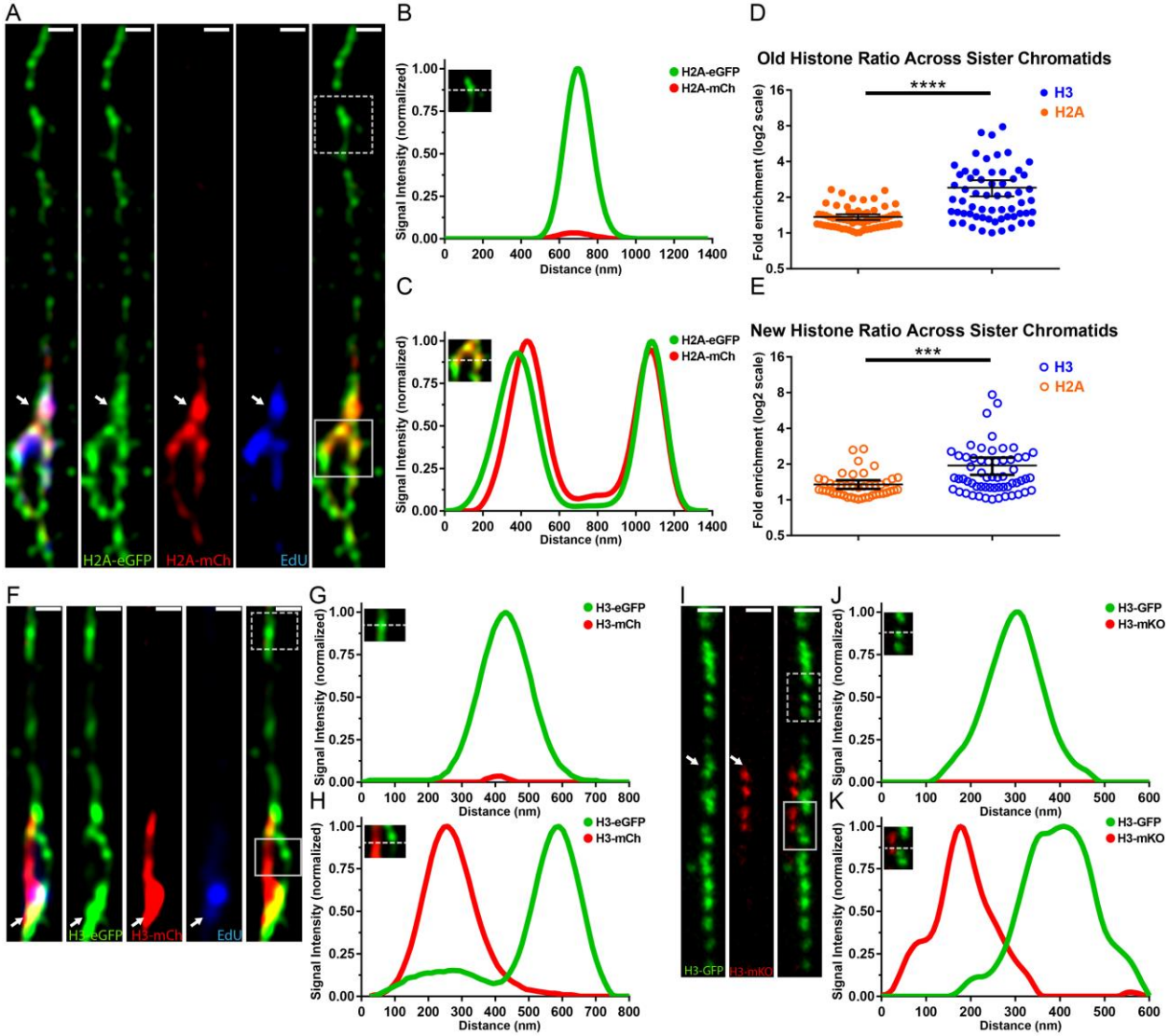

Figure 4: Asymmetric H3 and symmetric H2A distribution on replicating sister chromatids. (**A**) Airyscan image of chromatin fiber labelled with EdU showing old H2A-eGFP (green) and new H2A-mCherry (red) distribution on unreplicated and replicating regions. At the replicating region with EdU and new H2A signals, sister chromatids show symmetric old and new H2A distribution. Scale bar: 500nm. (**B**) Line-plot shows old H2A-eGFP and new H2A-mCherry distribution on unreplicated region without either EdU or new H2A (box with dotted

white lines in **A**, inset in **B**). (**C**) Line-plot shows old H2A-eGFP and new H2A-mCherry distribution on replicated region with both EdU and new H2A (box with solid white lines in **A**, inset in **C**). (**D**) Quantification of old H2A (n=65) and old H3 (n=61) distribution between sister chromatids at replication regions on chromatin fibers. (**E**) Quantification of new H2A (n=45) and new H3 (n=59) distribution between sister chromatids at replication regions on chromatin fibers. **** P< 0.0001, *** P< 0.001, Mann-Whitney U test. (**F**) Airyscan image of chromatin fiber labelled with EdU showing old H3-eGFP (green) and new H3-mCherry (red) distribution on unreplicated and replicating regions. At the replicating region with EdU and new H3 signals, sister chromatids show asymmetric old and new H3 distribution. Scale bar: 500nm. (**G**) Line-plot shows old H3-eGFP and new H3-mCherry distribution on unreplicated region without either EdU or new H3 (box with dotted white lines in **F**, inset in **G**). (**H**) Line-plot shows old H3-eGFP and new H3-mCherry distribution on replicated region with both EdU and new H3 (box with solid white lines in **F**, inset in **H**). (**I**) Two-color STED image of chromatin fiber showing old H3-GFP and new H3-mKO distribution on unreplicated and replicating chromatin region. New H3 incorporation is confined to regions that show double fiber indicative of replicating region. The transition from single fiber to double fiber is at the point where new histone incorporation begins (white arrow). (**J**) Line-plot shows old H3-GFP and new H3-mKO distribution on unreplicated region without new H3 (box with dotted white lines in **I**, inset in **J**). (**K**) Line-plot shows old H3-GFP and new H3-mKO distribution on replicated region with new H3 (box with solid white lines in **I**, inset in **K**).

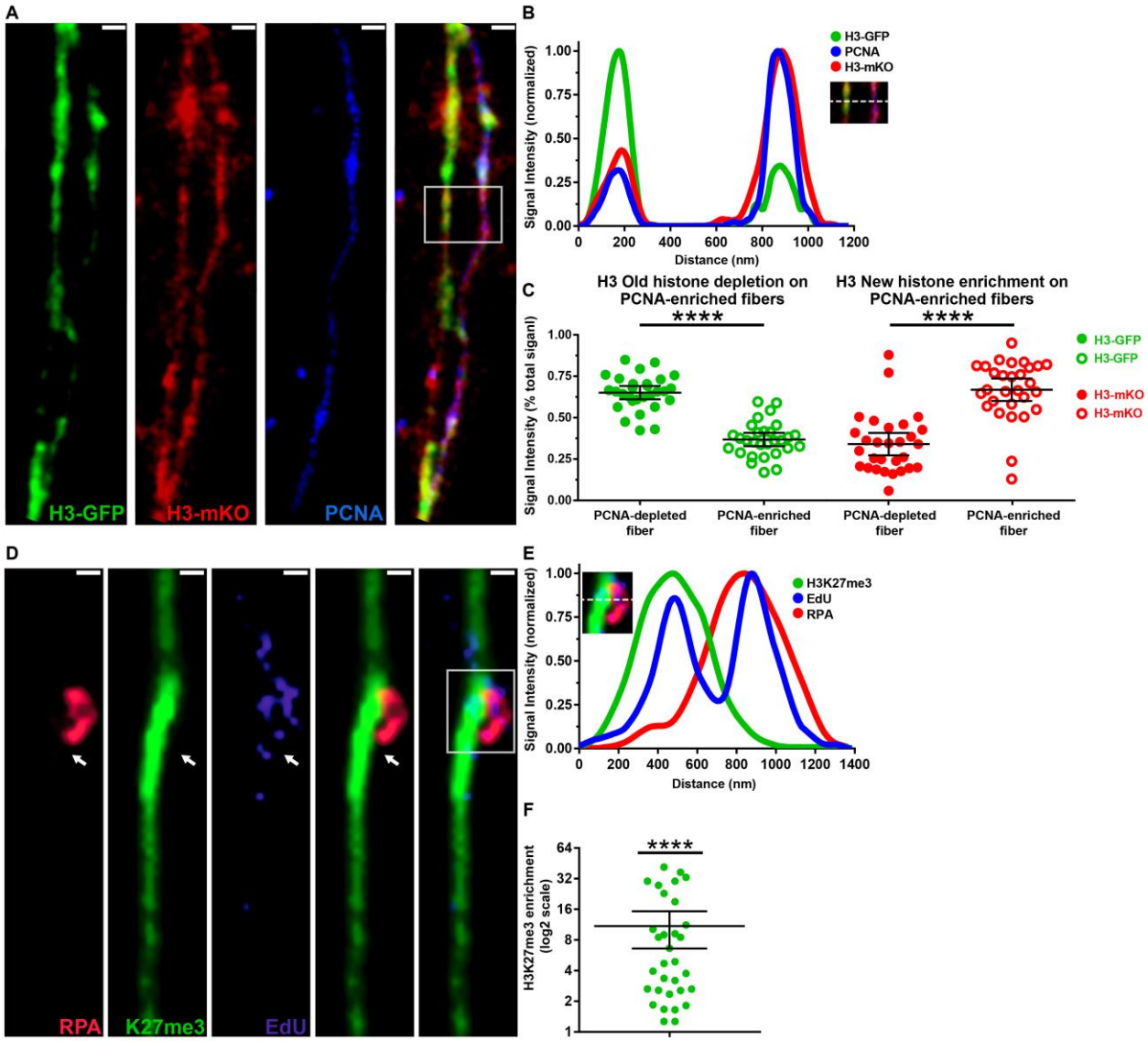

Figure 5: Old H3 preferentially associate with the leading strand while new H3 preferentially associate with the lagging strand on chromatin fibers. (**A**) STED image of chromatin fiber showing old and new H3 distribution on replicated chromatin fibers that incorporate new H3 throughout the fibers. One sister chromatid (to the right side) shows more PCNA than the other sister chromatid (to the left side). The PCNA-enriched strand is identified as the lagging strand. Old H3 show enriched signal on the leading (PCNA-depleted) strand. Scale bar: 500nm. (**B**) Line-plot shows PCNA, old H3-GFP and new H3-mKO distribution across replicated region (box with solid white lines in **A**, inset in **B**). PCNA is co-enriched with

new H3-mKO but not with old H3-GFP. (**C**) Differential distribution of old H3 *versus* new H3 on sister chromatids either depleted or enriched with PCNA: Old H3 (n=29) is enriched on PCNA-depleted strand whereas new H3 (n=29) is enriched at PCNA-enriched strand. **** $P<$ 0.0001, Students t-test. (**D**) Confocal image of chromatin fiber labelled with EdU showing anti-correlated H3K27me3 and RPA distribution. The transition from single fiber to double fibers is correlated with the EdU incorporation site (white arrow). (**E**) Line-plot shows EdU, H3K27me3 and RPA distribution across replicating region (box with solid white lines in **D**, inset in **E**). (**F**) Quantification of the ratio= H3K27me3 on RPA-depleted sister chromatid/ H3K27me3 on RPA-enriched sister chromatid (n=31). Y-axis is with $\log_2$ scale. **** $P<$ 0.0001, Mann-Whitney U test.

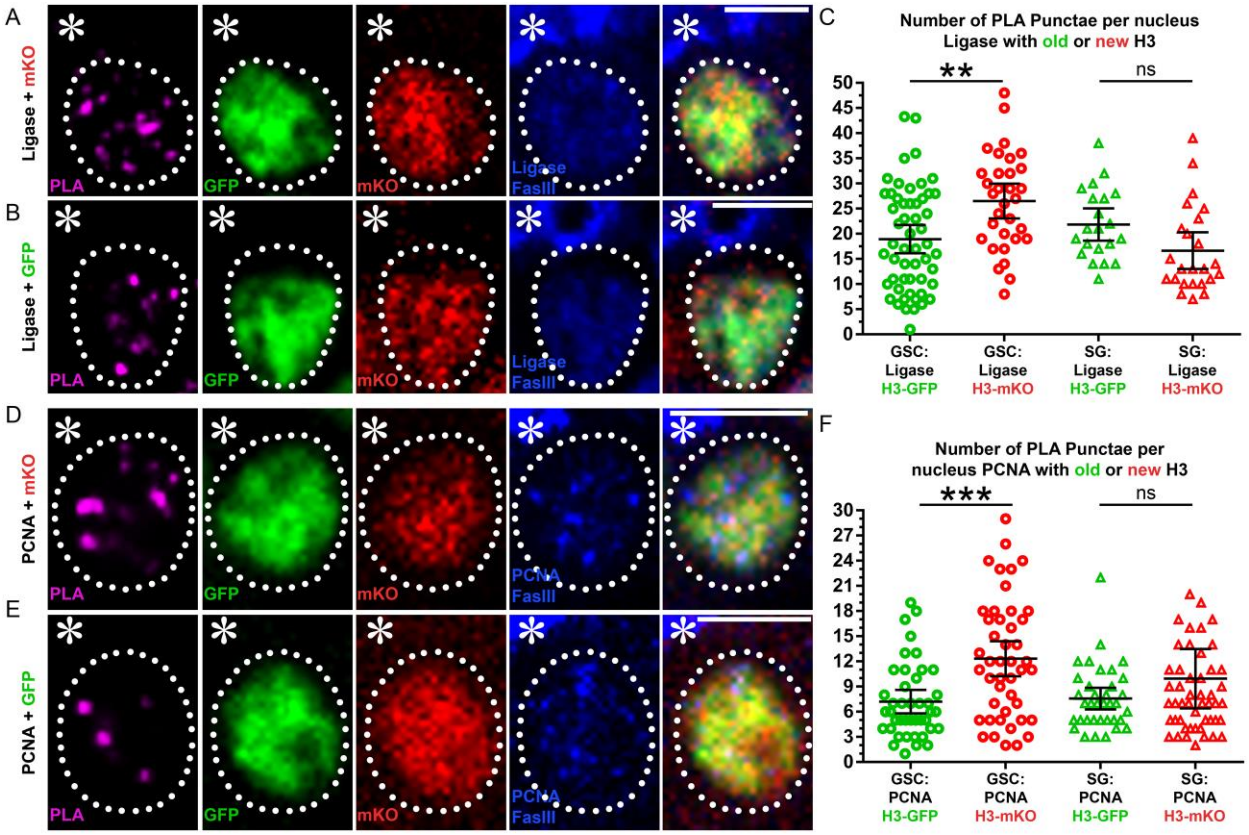

Figure 6: Proximity ligation assay shows distinct proximity between histones (old *versus* new) and lagging strand-enriched DNA replication machinery components in GSCs. (**A**) A representative GSC showing PLA signals (magenta) between lagging-strand-specific Ligase-HA (blue) and new H3-mKO (red). (**B**) A representative GSC showing PLA signals between Ligase-HA and old H3-GFP (green). (**C**) Quantification of the number of PLA puncta per nucleus between Ligase and histones (old *versus* new) in GSCs and SGs: In GSCs, PLA puntae between ligase and new H3-mKO: 26.5 ± 1.7, *n*=35; between ligase and old H3-GFP: 18.5 ± 2.5, *n*=53. In SGs, PLA puntae between ligase and new H3-mKO: 16.67±1.75, *n*=24; between ligase and old H3-GFP: 21.86±1.53, *n*=21. (**D**) A representative GSC showing PLA signals (magenta) between lagging-strand enriched PCNA (blue) and new H3-mKO (red). (**E**) A representative GSC showing PLA signals between PCNA and old H3-GFP (green). (**F**) Quantification of the number of PLA puncta per nucleus between PCNA and histones (old *versus* new) in GSCs and SGs: In

GSCs, PLA puntae between PCNA and new H3-mKO: 12.3 ± 1.0, *n*=46; between PCNA and old H3-GFP: 7.2 ± 0.7, *n*=42. In SGs, PLA puntae between PCNA and new H3-mKO: 9.96±1.76, *n*=50; between PCNA and old H3-GFP: 7.58±0.63, *n*=36. **: $P < 0.01$, ***: $P < 0.001$, Kruskal-Wallis multiple comparisons of non-parametric data with Dunn's multiple comparisons corrections test. Scale bar: 5μm.

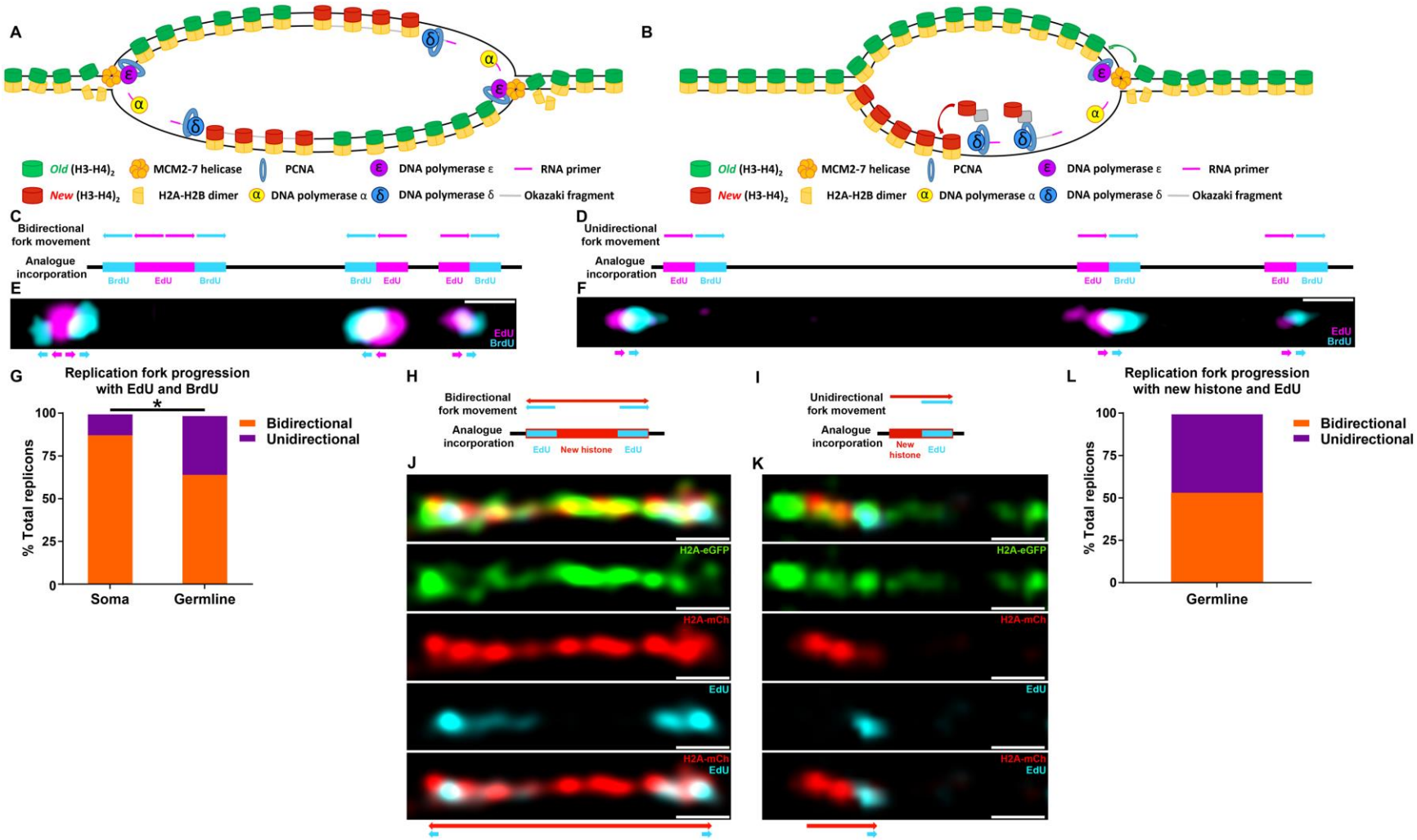

Figure 7: Germline-derived chromatin fibers show more unidirectional fork progression compared to soma-derived chromatin fibers. (**A**) A cartoon showing strand biased histone incorporation at a bidirectional replication fork. (**B**) A cartoon showing strand

biased histone incorporation at a unidirectional replication fork. (**C**) Predicted bidirectional fork progression result. (**D**) Predicted unidirectional fork progression result. (**E**) Bidirectional fork progression pattern from somatic cell derived chromatin fiber. Replicons show early label (EdU in magenta) flanked by late label (BrdU in cyan) on both sides. (**F**) Unidirectional fork progression pattern from germline-derived chromatin fiber. Replicons show alternation between early label (EdU in magenta) and late label (BrdU in cyan) along the chromatin fiber toward the same direction. (**G**) Quantification of fork progression patterns in somatic cell-derived *versus* germline-derived chromatin fibers. Germline-derived fibers show a significantly higher incidence of unidirectional fork progression: 43% in germline (n=31) *versus* 13% in soma (n=31), *: P< 0.01, Chi-squared test. Scale bar: 1μm. (**H**) Predicted bidirectional fork progression result based on new H2A and a short pulse of EdU. (**I**) Predicted unidirectional fork progression result. (**J**) Bidirectional fork progression pattern: Replicons show new H2A flanked by a pulse label (EdU in cyan) on both sides. (**K**) Unidirectional fork progression pattern: Replicons show the EdU pulse label from one side of new H2A signal along the chromatin fiber. (**L**) Quantification of fork progression patterns in germline-derived chromatin fibers. Germline-derived fibers show a significantly higher incidence of unidirectional fork progression: 48% in germline (n=33). Scale bar: 1μm.

AUTHOR CONTRIBUTIONS

Conceptualization, M.W., Z.N., X.Y., J.S., J.G., J.X. and X.C.; Methodology, M.W., Z.N., X.Y., J.S., J.G., J.X., and X.C.; Investigation, M.W., Z.N., X.Y., J.S., J-M. K., E.U., J.B.; Writing – Original Draft, M.W., Z.N., X.Y., J.S., J.G., J.X. and X.C.; Funding Acquisition, J.X., J.G. and X.C.; Supervision, J.X., J.G. and X.C.

ACKNOWLEDGMENTS

We thank B. Shelby and E. Wieschaus for the RPA-GFP fly line. We thank E. Moudrianakis, A. Spradling, J. Berger, M. Van Doren, R. Johnston and X.C. lab members for suggestions. We thank Johns Hopkins Integrated Imaging Center for confocal imaging and Carnegie Institute Imaging Center for STED microscopy work. Supported by NIH 5T32GM007231 and F31 GM115149-01A1 (M.W.), NIH R01GM112008 (J.X.), NIH R01 GM33397 (J.G.), NIH R01GM112008 and R35GM127075, the Howard Hughes Medical Institute, the Bill & Melinda Gates Foundation, the Simons Foundation, the David and Lucile Packard Foundation, and Johns Hopkins University startup funds (X.C.)

REFERENCES

Abdurashidova, G., Deganuto, M., Klima, R., Riva, S., Biamonti, G., Giacca, M., and Falaschi, A. (2000). Start sites of bidirectional DNA synthesis at the human lamin B2 origin. Science *287*, 2023-2026.

Ahmad, K., and Henikoff, S. (2002). Histone H3 variants specify modes of chromatin assembly. Proc Natl Acad Sci U S A *99 Suppl 4*, 16477-16484.

Alabert, C., Barth, T.K., Reveron-Gomez, N., Sidoli, S., Schmidt, A., Jensen, O.N., Imhof, A., and Groth, A. (2015a). Two distinct modes for propagation of histone PTMs across the cell cycle. Genes Dev *29*, 585-590.

Alabert, C., Barth, T.K., Reverón-Gómez, N., Sidoli, S., Schmidt, A., Jensen, O.N., Imhof, A., and Groth, A. (2015b). Two distinct modes for propagation of histone PTMs across the cell cycle. Genes & Development *29*, 585-590.

Alabert, C., and Groth, A. (2012). Chromatin replication and epigenome maintenance. Nat Rev Mol Cell Biol *13*, 153-167.

Alberts, B.M., Barry, J., Bedinger, P., Formosa, T., Jongeneel, C.V., and Kreuzer, K.N. (1983). Studies on DNA replication in the bacteriophage T4 in vitro system. Cold Spring Harb Symp Quant Biol *47 Pt 2*, 655-668.

Allis, C.D., and Jenuwein, T. (2016). The molecular hallmarks of epigenetic control. Nat Rev Genet *17*, 487-500.

Almouzni, G., Clark, D.J., Mechali, M., and Wolffe, A.P. (1990). Chromatin assembly on replicating DNA in vitro. Nucleic Acids Res *18*, 5767-5774.

Annunziato, A.T. (2013). Assembling chromatin: the long and winding road. Biochim Biophys Acta *1819*, 196-210.

Annunziato, A.T. (2015). The Fork in the Road: Histone Partitioning During DNA Replication. Genes (Basel) *6*, 353-371.

Annunziato, A.T., Schindler, R.K., Riggs, M.G., and Seale, R.L. (1982). Association of newly synthesized histones with replicating and nonreplicating regions of chromatin. J Biol Chem *257*, 8507-8515.

Bermek, O., Willcox, S., and Griffith, J.D. (2015). DNA Replication Catalyzed by Herpes Simplex Virus Type 1 Proteins Reveals Trombone Loops at the Fork. J Biol Chem *290*, 2539-2545.

Betschinger, J., and Knoblich, J.A. (2004). Dare to be different: asymmetric cell division in Drosophila, C. elegans and vertebrates. Curr Biol *14*, R674-685.

Blower, M.D., Sullivan, B.A., and Karpen, G.H. (2002). Conserved Organization of Centromeric Chromatin in Flies and Humans. Developmental Cell *2*, 319-330.

Blumenthal, A.B., Kriegstein, H.J., and Hogness, D.S. (1974). The units of DNA replication in Drosophila melanogaster chromosomes. Cold Spring Harb Symp Quant Biol *38*, 205-223.

Blythe, S.A., and Wieschaus, E.F. (2015). Zygotic genome activation triggers the DNA replication checkpoint at the midblastula transition. Cell *160*, 1169-1181.

Buck, S.W., Sandmeier, J.J., and Smith, J.S. (2002). RNA polymerase I propagates unidirectional spreading of rDNA silent chromatin. Cell *111*, 1003-1014.

Burgess, R.J., and Zhang, Z. (2013). Histone chaperones in nucleosome assembly and human disease. Nat Struct Mol Biol *20*, 14-22.

Burhans, W.C., Vassilev, L.T., Caddle, M.S., Heintz, N.H., and DePamphilis, M.L. (1990). Identification of an origin of bidirectional DNA replication in mammalian chromosomes. Cell *62*, 955-965.
Cairns, J. (1963). The bacterial chromosome and its manner of replication as seen by autoradiography. J Mol Biol *6*, 208-213.
Cairns, J. (1966). Autoradiography of HeLa cell DNA. J Mol Biol *15*, 372-373.
Clevers, H. (2005). Stem cells, asymmetric division and cancer. Nat Genet *37*, 1027-1028.
Cohen, S.M., Chastain, P.D., 2nd, Cordeiro-Stone, M., and Kaufman, D.G. (2009). DNA replication and the GINS complex: localization on extended chromatin fibers. Epigenetics Chromatin *2*, 6.
Cusick, M.E., DePamphilis, M.L., and Wassarman, P.M. (1984). Dispersive segregation of nucleosomes during replication of simian virus 40 chromosomes. J Mol Biol *178*, 249-271.
Dalgaard, J.Z., and Klar, A.J. (2001). A DNA replication-arrest site RTS1 regulates imprinting by determining the direction of replication at mat1 in S. pombe. Genes Dev *15*, 2060-2068.
Debyser, Z., Tabor, S., and Richardson, C.C. (1994). Coordination of leading and lagging strand DNA synthesis at the replication fork of bacteriophage T7. Cell *77*, 157-166.
Dunn, K., and Griffith, J.D. (1980). The presence of RNA in a double helix inhibits its interaction with histone protein. Nucleic Acids Res *8*, 555-566.
Fuller, M.T., and Spradling, A.C. (2007). Male and female Drosophila germline stem cells: two versions of immortality. Science *316*, 402-404.
Graham, J.E., Marians, K.J., and Kowalczykowski, S.C. (2017). Independent and Stochastic Action of DNA Polymerases in the Replisome. Cell *169*, 1201-1213 e1217.
Hamdan, S.M., Loparo, J.J., Takahashi, M., Richardson, C.C., and van Oijen, A.M. (2009). Dynamics of DNA replication loops reveal temporal control of lagging-strand synthesis. Nature *457*, 336-339.
Hand, R. (1975). Regulation of DNA replication on subchromosomal units of mammalian cells. J Cell Biol *64*, 89-97.
Hell, S.W., and Wichmann, J. (1994). Breaking the diffraction resolution limit by stimulated emission: stimulated-emission-depletion fluorescence microscopy. Opt Lett *19*, 780-782.
Horvath, P., and Barrangou, R. (2010). CRISPR/Cas, the immune system of bacteria and archaea. Science *327*, 167-170.
Huang, H., Stromme, C.B., Saredi, G., Hodl, M., Strandsby, A., Gonzalez-Aguilera, C., Chen, S., Groth, A., and Patel, D.J. (2015). A unique binding mode enables MCM2 to chaperone histones H3-H4 at replication forks. Nat Struct Mol Biol *22*, 618-626.
Huberman, J.A., and Riggs, A.D. (1968). On the mechanism of DNA replication in mammalian chromosomes. J Mol Biol *32*, 327-341.
Inaba, M., and Yamashita, Y.M. (2012). Asymmetric stem cell division: precision for robustness. Cell Stem Cell *11*, 461-469.
Jackson, V. (1988). Deposition of newly synthesized histones: hybrid nucleosomes are not tandemly arranged on daughter DNA strands. Biochemistry *27*, 2109-2120.
Jackson, V., and Chalkley, R. (1981a). A new method for the isolation of replicative chromatin: selective deposition of histone on both new and old DNA. Cell *23*, 121-134.
Jackson, V., and Chalkley, R. (1981b). A reevaluation of new histone deposition on replicating chromatin. J Biol Chem *256*, 5095-5103.
Jackson, V., and Chalkley, R. (1985). Histone segregation on replicating chromatin. Biochemistry *24*, 6930-6938.

Janke, R., King, G.A., Kupiec, M., and Rine, J. (2018). Pivotal roles of PCNA loading and unloading in heterochromatin function. Proc Natl Acad Sci U S A *115*, E2030-E2039.
Kadyrov, F.A., and Drake, J.W. (2002). Characterization of DNA synthesis catalyzed by bacteriophage T4 replication complexes reconstituted on synthetic circular substrates. Nucleic Acids Res *30*, 4387-4397.
Katan-Khaykovich, Y., and Struhl, K. (2011). Splitting of H3-H4 tetramers at transcriptionally active genes undergoing dynamic histone exchange. Proc Natl Acad Sci U S A *108*, 1296-1301.
Ke, M.T., Nakai, Y., Fujimoto, S., Takayama, R., Yoshida, S., Kitajima, T.S., Sato, M., and Imai, T. (2016). Super-Resolution Mapping of Neuronal Circuitry With an Index-Optimized Clearing Agent. Cell Rep *14*, 2718-2732.
Kimura, H. (2005). Histone dynamics in living cells revealed by photobleaching. DNA Repair (Amst) *4*, 939-950.
Kouzarides, T. (2007). Chromatin modifications and their function. Cell *128*, 693-705.
Krude, T., and Knippers, R. (1991). Transfer of nucleosomes from parental to replicated chromatin. Mol Cell Biol *11*, 6257-6267.
Lasko, P.F., and Ashburner, M. (1990). Posterior localization of vasa protein correlates with, but is not sufficient for, pole cell development. Genes Dev *4*, 905-921.
Lee, J., Chastain, P.D., Kusakabe, T., Griffith, J.D., and Richardson, C.C. (1998). Coordinated Leading and Lagging Strand DNA Synthesis on a Minicircular Template. Molecular Cell *1*, 1001-1010.
Lee, J.B., Hite, R.K., Hamdan, S.M., Xie, X.S., Richardson, C.C., and van Oijen, A.M. (2006). DNA primase acts as a molecular brake in DNA replication. Nature *439*, 621-624.
Leffak, I.M., Grainger, R., and Weintraub, H. (1977). Conservative assembly and segregation of nucleosomal histones. Cell *12*, 837-845.
Li, J.J., and Kelly, T.J. (1985). Simian virus 40 DNA replication in vitro: specificity of initiation and evidence for bidirectional replication. Mol Cell Biol *5*, 1238-1246.
Lin, S., Yuan, Z.F., Han, Y., Marchione, D.M., and Garcia, B.A. (2016). Preferential Phosphorylation on Old Histones during Early Mitosis in Human Cells. J Biol Chem *291*, 15342-15357.
Martin-Parras, L., Hernandez, P., Martinez-Robles, M.L., and Schvartzman, J.B. (1991). Unidirectional replication as visualized by two-dimensional agarose gel electrophoresis. J Mol Biol *220*, 843-853.
McKnight, S.L., and Miller, O.L., Jr. (1977). Electron microscopic analysis of chromatin replication in the cellular blastoderm Drosophila melanogaster embryo. Cell *12*, 795-804.
Merrick, C.J., Jackson, D., and Diffley, J.F. (2004). Visualization of altered replication dynamics after DNA damage in human cells. J Biol Chem *279*, 20067-20075.
Morrison, S.J., and Kimble, J. (2006). Asymmetric and symmetric stem-cell divisions in development and cancer. Nature *441*, 1068-1074.
Nieminuszczy, J., Schwab, R.A., and Niedzwiedz, W. (2016). The DNA fibre technique - tracking helicases at work. Methods *108*, 92-98.
Petruk, S., Sedkov, Y., Johnston, D.M., Hodgson, J.W., Black, K.L., Kovermann, S.K., Beck, S., Canaani, E., Brock, H.W., and Mazo, A. (2012). TrxG and PcG proteins but not methylated histones remain associated with DNA through replication. Cell *150*, 922-933.
Prelich, G., and Stillman, B. (1988). Coordinated leading and lagging strand synthesis during SV40 DNA replication in vitro requires PCNA. Cell *53*, 117-126.

Riley, D., and Weintraub, H. (1979). Conservative segregation of parental histones during replication in the presence of cycloheximide. Proc Natl Acad Sci U S A *76*, 328-332.
Roufa, D.J., and Marchionni, M.A. (1982). Nucleosome segregation at a defined mammalian chromosomal site. Proc Natl Acad Sci U S A *79*, 1810-1814.
Russev, G., and Hancock, R. (1981). Formation of hybrid nucleosomes cantaining new and old histones. Nucleic Acids Res *9*, 4129-4137.
Sasaki, T., Sawado, T., Yamaguchi, M., and Shinomiya, T. (1999). Specification of regions of DNA replication initiation during embryogenesis in the 65-kilobase DNApolalpha-dE2F locus of Drosophila melanogaster. Mol Cell Biol *19*, 547-555.
Seale, R.L. (1976). Studies on the mode of segregation of histone nu bodies during replication in HeLa cells. Cell *9*, 423-429.
Seidman, M.M., Levine, A.J., and Weintraub, H. (1979). The asymmetric segregation of parental nucleosomes during chrosome replication. Cell *18*, 439-449.
Sheng, X.R., and Matunis, E. (2011). Live imaging of the Drosophila spermatogonial stem cell niche reveals novel mechanisms regulating germline stem cell output. Development *138*, 3367-3376.
Snedeker, J., Wooten, M., and Chen, X. (2017). The Inherent Asymmetry of DNA Replication. Annu Rev Cell Dev Biol *33*, 291-318.
Sogo, J.M., Stahl, H., Koller, T., and Knippers, R. (1986). Structure of replicating simian virus 40 minichromosomes. The replication fork, core histone segregation and terminal structures. J Mol Biol *189*, 189-204.
Spradling, A., Fuller, M.T., Braun, R.E., and Yoshida, S. (2011). Germline stem cells. Cold Spring Harb Perspect Biol *3*, a002642.
Stano, N.M., Jeong, Y.J., Donmez, I., Tummalapalli, P., Levin, M.K., and Patel, S.S. (2005). DNA synthesis provides the driving force to accelerate DNA unwinding by a helicase. Nature *435*, 370-373.
Stengel, G., and Kuchta, R.D. (2011). Coordinated Leading and Lagging Strand DNA Synthesis by Using the Herpes Simplex Virus 1 Replication Complex and Minicircle DNA Templates. J Virol *85*, 957-967.
Sugasawa, K., Ishimi, Y., Eki, T., Hurwitz, J., Kikuchi, A., and Hanaoka, F. (1992). Nonconservative segregation of parental nucleosomes during simian virus 40 chromosome replication in vitro. Proc Natl Acad Sci U S A *89*, 1055-1059.
Tarayrah, L., and Chen, X. (2013). Epigenetic regulation in adult stem cells and cancers. Cell Biosci *3*, 41.
Tittel-Elmer, M., Lengronne, A., Davidson, M.B., Bacal, J., Francois, P., Hohl, M., Petrini, J.H.J., Pasero, P., and Cobb, J.A. (2012). Cohesin association to replication sites depends on rad50 and promotes fork restart. Mol Cell *48*, 98-108.
Tran, V., Feng, L., and Chen, X. (2013). Asymmetric distribution of histones during Drosophila male germline stem cell asymmetric divisions. Chromosome Res *21*, 255-269.
Tran, V., Lim, C., Xie, J., and Chen, X. (2012). Asymmetric division of Drosophila male germline stem cell shows asymmetric histone distribution. Science *338*, 679-682.
Verreault, A. (2003). Histone Deposition at the Replication Fork: A Matter of Urgency. Molecular Cell *11*, 283-284.
Weintraub, H. (1976). Cooperative alignment of nu bodies during chromosome replication in the presence of cycloheximide. Cell *9*, 419-422.

Wold, M.S. (1997). Replication protein A: a heterotrimeric, single-stranded DNA-binding protein required for eukaryotic DNA metabolism. Annu Rev Biochem *66*, 61-92.
Wolstenholme, D.R. (1973). Replicating DNA molecules from eggs of Drosophila melanogaster. Chromosoma *43*, 1-18.
Worcel, A., Han, S., and Wong, M.L. (1978). Assembly of newly replicated chromatin. Cell *15*, 969-977.
Wright, A.V., Nunez, J.K., and Doudna, J.A. (2016). Biology and Applications of CRISPR Systems: Harnessing Nature's Toolbox for Genome Engineering. Cell *164*, 29-44.
Wu, H., and Sun, Y.E. (2006). Epigenetic regulation of stem cell differentiation. Pediatr Res *59*, 21R-25R.
Wutz, A. (2013). Epigenetic regulation of stem cells : the role of chromatin in cell differentiation. Adv Exp Med Biol *786*, 307-328.
Xie, J., Wooten, M., Tran, V., Chen, B.C., Pozmanter, C., Simbolon, C., Betzig, E., and Chen, X. (2015). Histone H3 Threonine Phosphorylation Regulates Asymmetric Histone Inheritance in the Drosophila Male Germline. Cell *163*, 920-933.
Xie, J., Wooten, M., Tran, V., and Chen, X. (2017). Breaking Symmetry - Asymmetric Histone Inheritance in Stem Cells. Trends Cell Biol *27*, 527-540.
Xu, M., Long, C., Chen, X., Huang, C., Chen, S., and Zhu, B. (2010). Partitioning of histone H3-H4 tetramers during DNA replication-dependent chromatin assembly. Science *328*, 94-98.
Yadlapalli, S., Cheng, J., and Yamashita, Y.M. (2011). Drosophila male germline stem cells do not asymmetrically segregate chromosome strands. J Cell Sci *124*, 933-939.
Yadlapalli, S., and Yamashita, Y.M. (2013). Chromosome-specific nonrandom sister chromatid segregation during stem-cell division. Nature.
Yang, J., Nelson, S.W., and Benkovic, S.J. (2006). The control mechanism for lagging strand polymerase recycling during bacteriophage T4 DNA replication. Mol Cell *21*, 153-164.
Yao, N.Y., Georgescu, R.E., Finkelstein, J., and O'Donnell, M.E. (2009). Single-molecule analysis reveals that the lagging strand increases replisome processivity but slows replication fork progression. Proc Natl Acad Sci U S A *106*, 13236-13241.
Yeeles, J.T., and Marians, K.J. (2013). Dynamics of leading-strand lesion skipping by the replisome. Mol Cell *52*, 855-865.
Young, N.L., DiMaggio, P.A., and Garcia, B.A. (2010). The significance, development and progress of high-throughput combinatorial histone code analysis. Cellular and Molecular Life Sciences *67*, 3983-4000.
Yu, C., Gan, H., Han, J., Zhou, Z.X., Jia, S., Chabes, A., Farrugia, G., Ordog, T., and Zhang, Z. (2014). Strand-specific analysis shows protein binding at replication forks and PCNA unloading from lagging strands when forks stall. Mol Cell *56*, 551-563.
Zheng, G., Kanchwala, M., Xing, C., and Yu, H. (2018). MCM2-7-dependent cohesin loading during S phase promotes sister-chromatid cohesion. Elife *7*.

SUPPLEMENTAL INFORMATION

EXPERIMENTAL PROCEDURES

Chromatin fiber preparation with nucleoside analogue incorporation and immunostaining

Testes were dissected in warm Schneider's media. Once dissection was accomplished, testes were transferred to Schneider's medium containing 20μM EdU analogue. Testes were incubated for 30 minutes, rotating, at room temperature unless otherwise specified in the protocol. At the end of the 30 minutes, Schneider media was drained and testes samples were washed three times in lysis buffer (80mM NaCl, 150mM Tris-base, 0.2% Joy detergent, pH 10). Testes were transferred to clean glass slide and residual lysis buffer was drained off. Then 20μl of lysis buffer were added to the slide to immerse the testis samples. Testis were manually broken apart with dissecting forceps and allowed to sit in lysis buffer until cells were fully lysed (~5 minutes). 10μl of sucrose/formalin solution (1M sucrose; 10% formaldehyde) was then added and lysed sample was let sit for 5 minutes. A large coverslip (24x60mm) was then placed on top of the lysed chromatin solution and transferred immediately to liquid nitrogen and sit for two minutes. Cover slip was removed with razor blade, after which slide was transferred to cold (-20°C) 95% ethanol for 10 minutes. Next, slide was incubated with fixative solution [0.5% formaldehyde in 1xPBST (0.1% Triton)] for 30 seconds. Slides were drained and placed into coplin jar containing 50ml 1xPBS. Slides were washed twice by replacing the buffer. Slides were then placed in humidity chamber and pre-blocked with 1ml of blocking solution (2% BSA, PBS with 0.1% Triton) for 30 minutes. Blocking buffer was then drained and primary antibodies were added for incubation overnight at 4°C. Slides were then washed twice and incubated with secondary antibodies for two hours at room temperature. Slides were then washed twice and mounted with mounting media.

Note: For BrdU: Fibers were treated with 1M HCL for one hour at 37°C to expose BrdU epitope prior to addition of anti-BrdU primary antibody. For EdU visualization: EdU analogue was conjugated to Alexa-647 dye *via* CLICK chemistry [reviewed by (Kolb et al., 2001; Moses and Moorhouse, 2007)].

Superresolution STED imaging

Superresolution images were acquired using a Leica TCS SP8 STED microscope with a 1.4 NA 100X STED White objective. Antibody staining enhanced specimen brightness and photostability for STED. Secondary antibody fluorophore conjugates were empirically selected for STED performance and optimal 3-colour separation with the 592 nm continuous wave (CW) and 775 nm pulsed depletion lasers (Alexa 488 with STED 592nm, Alexa 568 with STED 775nm, and Alexa 647 with STED 775nm). Images were acquired as single z-planes for all tissue types; whole mount, squash and fiber preparations to minimize drift between channel acquisitions. Specimens included 100 nm TetraSpeck microsphere beads as fiducial markers (Thermo Fisher Catalog No. T7279). Instrument aberration and blurring was corrected with post-acquisition deconvolution using the Scientific Volume Imagine (SVI) Huygens Professional software package, which achieves improved calculated/theoretical PSFs via complete integration with the Leica LAS-X software and hardware. Detailed instrument acquisition and post-processing settings are available upon request.

PLA Assay

Following incubation with primary antibodies, proximity ligation assay (PLA; Olink) was performed using 20 µL of reaction per step per slide according to Sigma-Aldrich® Duolink®

In Situ PLA® manufacturer's instruction. In brief, two PLA secondary probes, anti-mouse MINUS (targeting anti-HA mouse primary) and anti-rabbit PLUS (targeting anti-GFP or anti-mKO rabbit primaries), were diluted 1:5 in Ab Diluent buffer provided by manufacturer and incubated overnight at 4 °C. Slides were washed in 1X wash buffer A for 10 minutes, followed by the ligation reaction, in which PLA ligation stock was diluted 1:5 in dH_2O and 1:40 ligase was added and incubated for 1hr at 37 °C. Slides were washed in wash buffer A for 5 minutes, followed by addition of the PLA amplification reaction (1:5 amplification stock and 1:80 polymerase diluted in dH_2O) covered for 2 hours at 37 °C. Slides were washed with 1X wash buffer B for 10 mins and 0.01X wash buffer B for 1 minute. Slides were then washed once in 1X PBS. Anti-mouse secondary was added (Alexa Fluor 405; 1:1000 Molecular Probes®) Images were taken using the Zeiss LSM 700 Multiphoton confocal microscope with a 63× oil immersion objectives and processed using Adobe Photoshop software.

Fly strains and husbandry

Fly stocks were raised using standard Bloomington medium at 18°C, 25°C, or 29°C as noted. The following fly stocks were used: *hs-flp* on the X chromosome (Bloomington Stock Center BL-26902), *nos-Gal4* on the 2nd chromosome (Van Doren et al., 1998), *UASp-FRT-H3-GFP-PolyA-H3-mKO* on the 3rd chromosome and *UASp-FRT-H2B-GFP-PolyA-H2B-mKO*, as reported previously (Tran et al., 2012). Other new histone transgenic strains generated for this work are described as follows and are all on either the 2nd or the 3rd chromosome as a single-copy transgene.

Generation of fly strains with different switchable dual-color transgenes

Standard procedures were used for all molecular cloning experiments. Enzymes used for plasmid construction were obtained from New England Biolabs (Beverly, MA). The new histone sequences, including *histone-mKO*, *histone-mCherry* or *histone-GFP*, were recovered as an XbaI flanked fragment and were subsequently inserted into the XbaI site of the UASp plasmid to construct the *UASp-new histone* plasmid. The old histone sequences, including *histone-GFP*, *histone-EGFP*, or *histone-mKO*, were inserted to *pBluescript-FRT-NheI-SV40 PolyA-FRT* plasmid at the unique NheI site. The entire *NotI-FRT-old histone-SV40 PolyA-FRT-EcoRI* sequences were then subcloned into the *UASp-new histone* plasmid digested by *NotI* and *EcoRI*. The final *UASp-FRT-old histone-PolyA-FRT-new histone* plasmids were introduced to w^{1118} flies by P-element-mediated germline transformation (Bestgene Inc.). Transgenic flies with the following transgenes were newly generated in studies reported here: *UASp-FRT-H4-GFP-PolyA-FRT-H4-mKO*, *UASp-FRT-H2A-GFP-PolyA-FRT-H2A-mKO*, *UASp-FRT-H2A-EGFP-PolyA-FRT-H2A-mCherry*, *UASp-FRT-H1-GFP-PolyA-FRT-H1-mKO*, *UASp-FRT-H3-mKO-PolyA-FRT-H3-GFP*, and *UASp-FRT-H3-EGFP-PolyA-FRT-H3-mCherry*.

Generating knock-in fly strains to tag genes encoding key DNA replication components

In collaboration with Fungene Inc. (Beijing, China), the following fly line was generated using the CRISPR-Cas9 technology: CG5602 (DNA ligase I, major replicative ligase) with 3xHA tag at the 3' immediately upstream of the STOP codon, generating the fusion protein: DNA ligase-3HA.

Heat shock scheme

Flies with *UASp*-dual color histone transgenes were paired with *nos-Gal4* drivers. Flies were raised at 25°C throughout development until adulthood to avoid pre-flipping.

For adult males: Before heat shock, 0-3 day old males were transferred to vials that had been air dried for 24 hours. Vials were submerged underneath water up to the plug in a circulating 37°C water bath for 90 minutes and recovered in a 29°C incubator for indicated time before dissection, followed by immunostaining or live cell imaging experiments.

For wandering third-instar larvae: bottles containing third instar larvae (pre-wandering stage) were submerged underneath water up to the plug in a circulating 37°C water bath for 90 minutes and recovered in a 29°C incubator for indicated time before dissection, followed by fiber preparation and immunostaining experiments.

Immunostaining experiments

Immunofluorescence staining was performed using standard procedures (Hime et al., 1996; Tran et al., 2012). Primary antibodies used were mouse anti-Fas III (1:200, DSHB, 7G10), anti-HA (1:200; Sigma-Aldrich H3663), anti-PCNA (1:200; Santa Cruz sc-56), anti-GFP (1:1,000; Abcam ab 13970), anti-mKO (1:200; MBL PM051M), and anti-BrdU (1:200; Abcam ab6326). BrdU analogue was Invitrogen B23151 5-bromo-2´-deoxyuridine (BrdU). Secondary antibodies were the Alexa Fluor-conjugated series (1:1000; Molecular Probes). Confocal images for immunostained fixed sample were taken using Zeiss LSM 700 Multiphoton confocal microscope with 63x or 100x oil immersion objectives and processed using Adobe Photoshop software.

EdU incorporation to label GSC-GB pair at S-phase

To avoid quantifying cells which become arrested and fail to progress throughout the cell cycle following heat shock, we utilized EdU, a thymidine analogue which can label cells actively undergoing DNA replication. EdU labeling of the GSC-GB pairs at S phase was performed using Click-iT Plus EdU Alexa Fluor 647 Imaging Kit (Life Science C10640) according to manufacturer's instructions. Dissected testes were immediately incubated in S2 medium with 100 μM EdU for 30 minutes at room temperature. The testes were subsequently fixed and proceed to primary antibody incubation. Fluorophore conjugation to EdU was performed along manufacturer's instructions and followed by secondary antibody incubation.

Quantification of GFP and mKO intensity in whole testis

No antibody was added to enhance either GFP or mKO signal. Values of GFP and mKO intensity were calculated using Image J software: DAPI signal was used to determine the area of nucleus for measuring both GFP and mKO fluorescent signals, the raw reading was subsequently adjusted by subtracting fluorescence signals in the hub region used as background in both GSC and GB nuclei and compared between each other.

Quantification of proteins on sister chromatids

To capture localized distribution of histones and other proteins on chromatin fibers, fibers were divided into 2μm segments along the length of both sister fibers. Two microns was chosen as this was the average size of individual replicons with 10 minute EdU pulses (Figure S4). Assuming a DNA polymerase rate of 1-1.5 kb/min, these regions likely represent ~10-15 kb of DNA. To

effectively compare histone distribution patterns across multiple sets of doublet fiber segments, we normalized fiber data using the following strategy to obtain ratio between the two sisters: First, we quantified fluorescence levels for both old histone (GFP or EGFP) and new histone (mKO or mCherry) for each singlet fiber segment making up the doublet fiber segment. We then divided the singlet fiber segment with greater fluorescence intensity by the singlet fiber segment with less fluorescence intensity to generate a ratio of the relative difference in histone enrichment levels.

Supplementary Figures and Figure Legends:

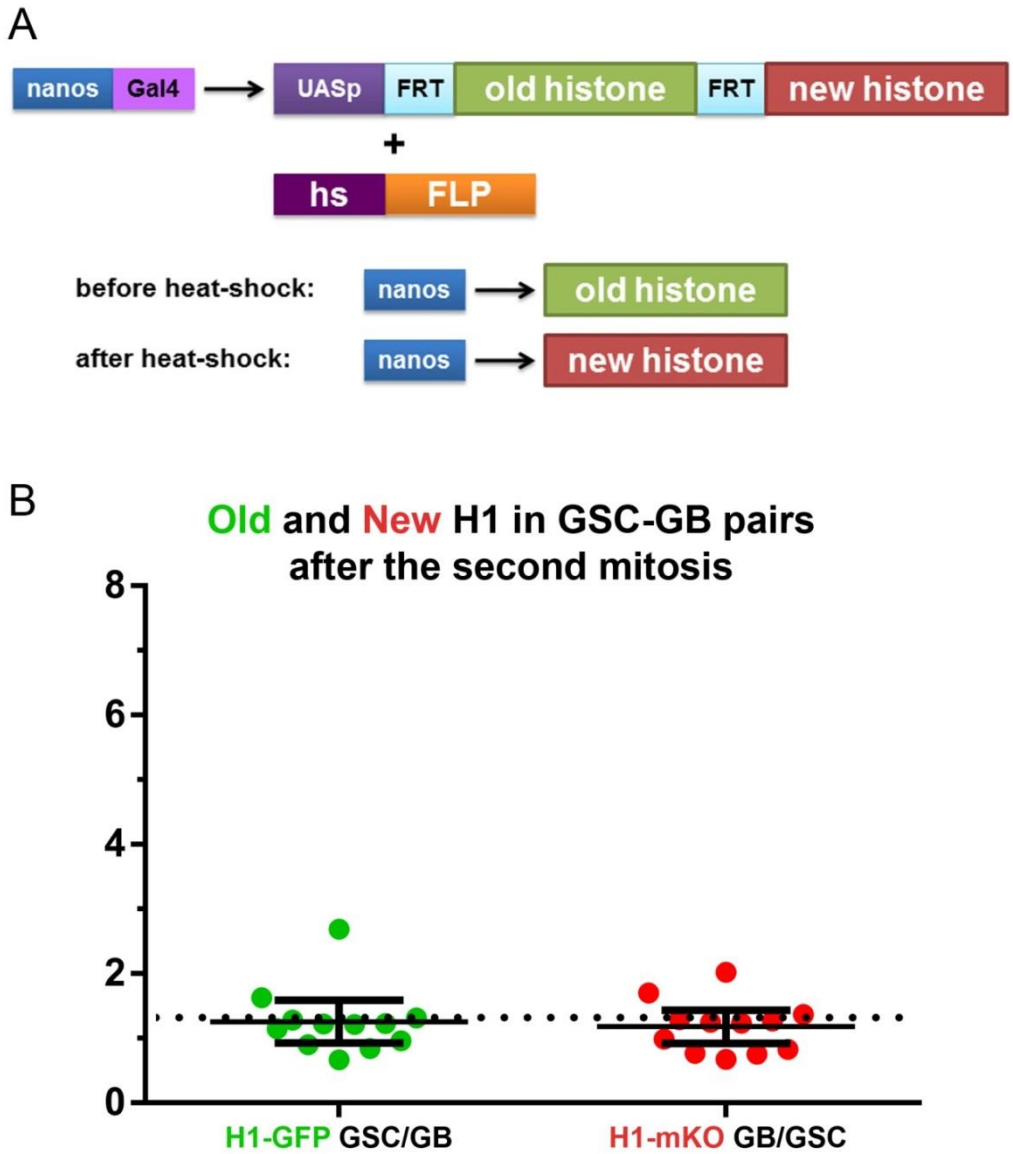

Figure S1: (**A**) A schematic diagram showing the dual color switch design that expresses pre-existing histone and newly synthesized histone by heat-shock treatment, as adapted from (Tran et al., 2012). (**B**) Histone H1 showed overall symmetric inheritance pattern in post-mitotic GSC-GB pairs (n=12). See Table S4 for details. Neither old H1 nor new H1 is significantly different from the value of 1; P = 0.092 for old H1; P = 0.151 for new H1, based on Wilcoxon signed rank test.

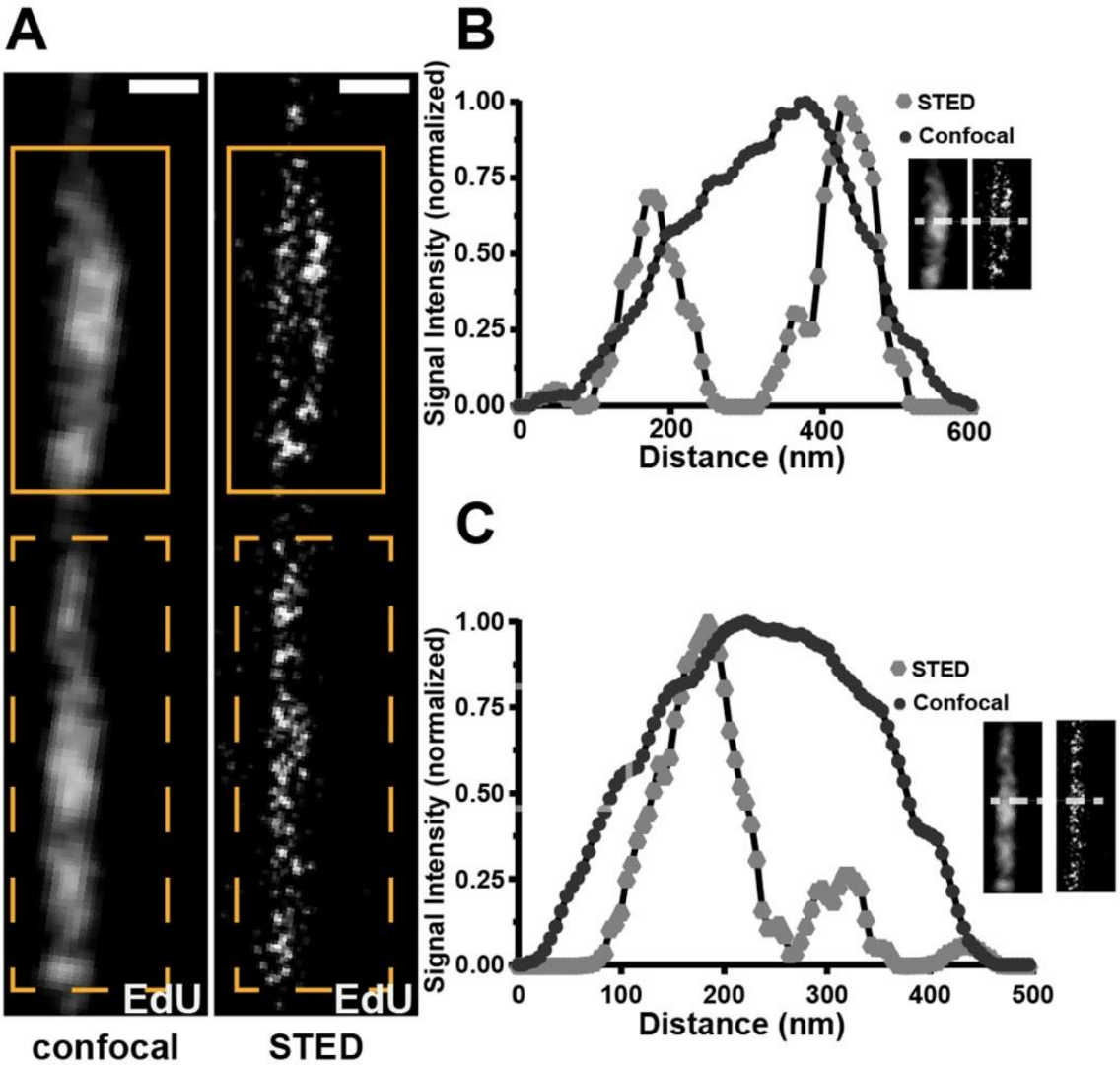

Figure S2: (**A**) Confocal *versus* STED images to compare EdU signals on replicating chromatin fiber. Neither region (box with solid orange lines and box with dotted orange lines) can be resolved with confocal. (**B**) Upper region (box with solid orange lines in **A**, inset in **B**) can be resolved into two sister chromatids with STED. Line-plot shows a single fiber structure with confocal but double fiber structure with STED. (**C**) Lower region (box with dotted orange lines in **A**, inset in **C**) cannot be resolved with STED, likely due to tight cohesion between sister chromatids. Line-plot shows mainly a single fiber structure with both confocal and STED.

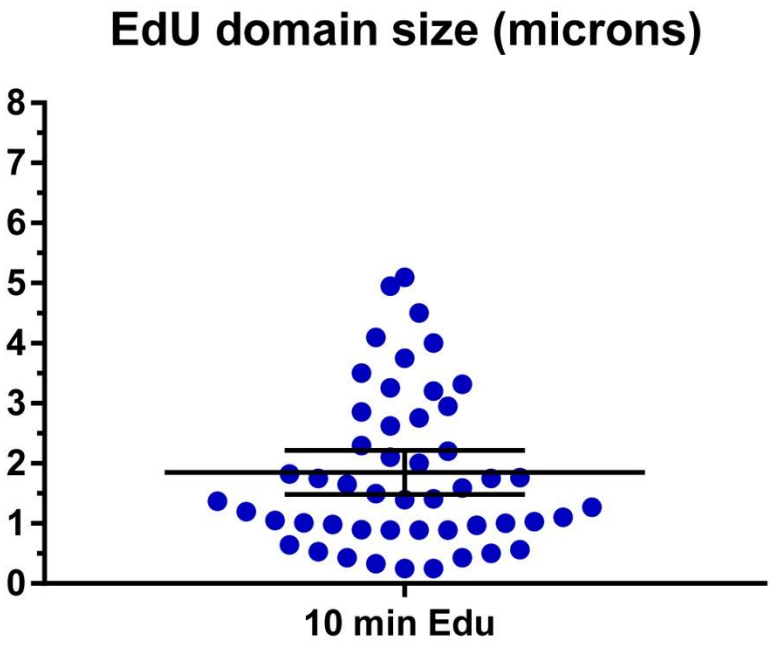

Figure S3: Size of chromatin fiber pulsed with 10-minute EdU. The 10 minute EdU-pulse is the shortest length of time that we could get reliable and clear EdU signals on isolated fibers, which yields on average 2μm-long chromatin fibers. If we assume a DNA polymerase rate is 1-1.5 kb per min, a 2μm stretch on fiber represents approximately 10-15 kb-DNA fragment.

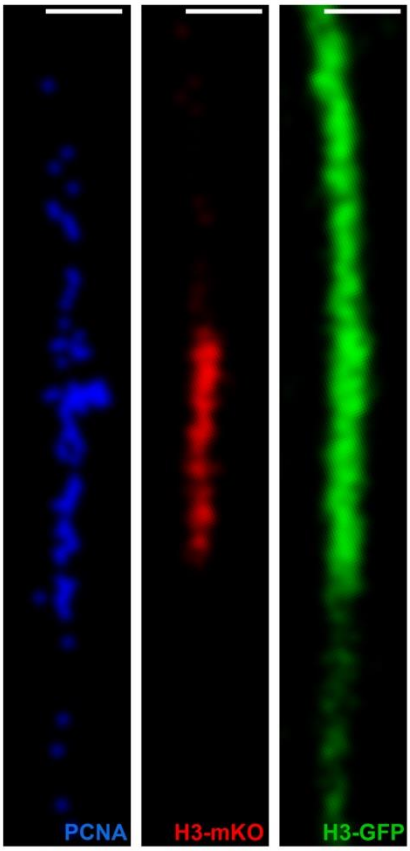

Figure S4: Chromatin fiber stained with for old H3 using anti-GFP (green), new H3 using anti-mKO (red), and a DNA replication machinery component PCNA using anti-PCNA (blue). Confocal images show PCNA, new histone (H3-mKO) and old histone (H3-GFP) along a chromatin fiber. New histone incorporation is confined to the PCNA-positive region along the chromatin fiber. Scale bar: 1μm.

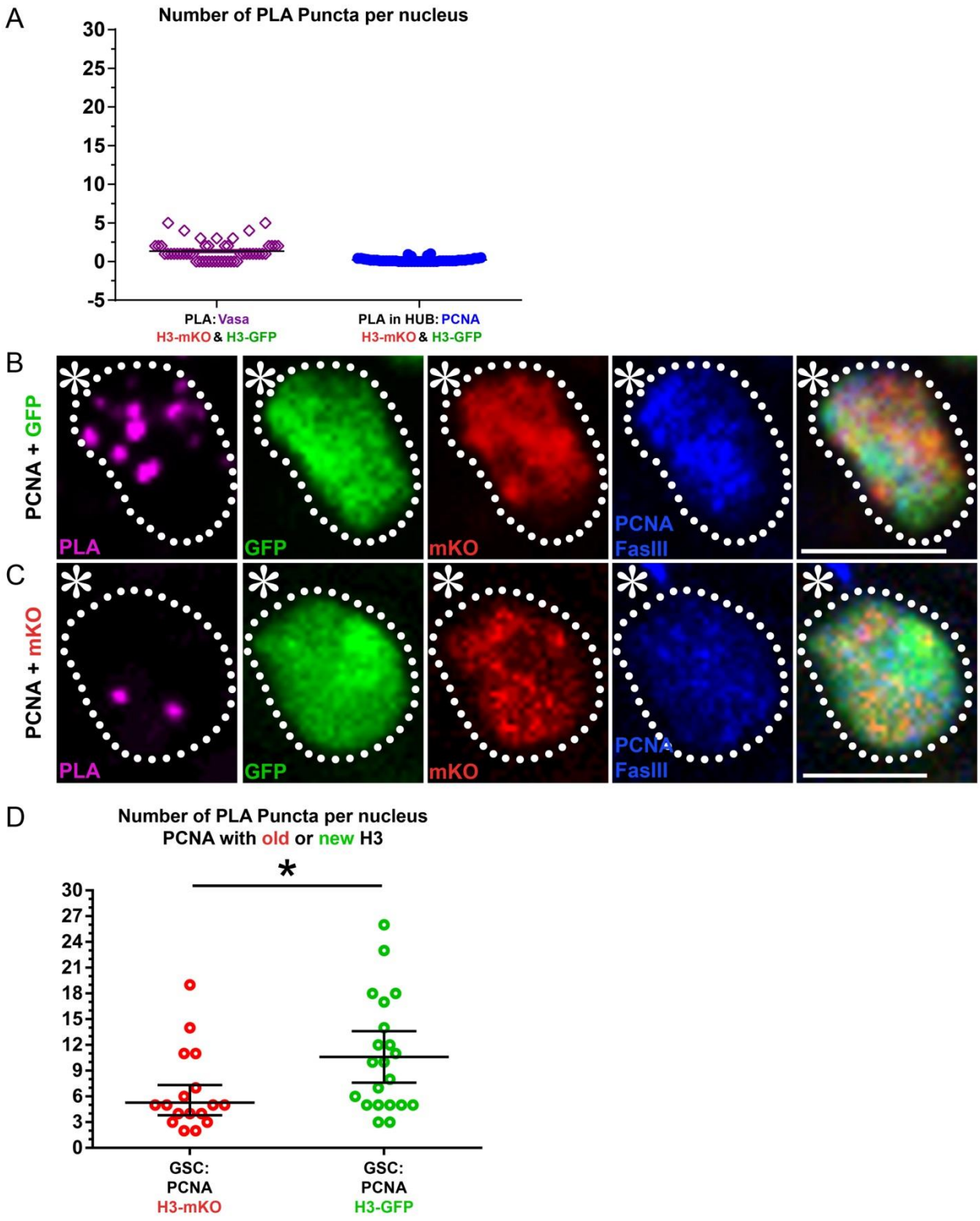

Figure S5: Control experiments for the PLA experiments. (**A**) Quantification of PLA signals in two negative control experiments: first, PLA experiments were performed between histones

and a cytoplasmic protein Vasa; second, PLA signals were counted in non-replicating somatic hub cells**.** Both showed very low signals. (**B-D**) PLA signals between new H3 labeled with GFP and the lagging strand-enriched component PCNA (**B**) *versus* between old histone H3 labeled with mKO and the lagging strand-enriched component PCNA (**C**). (**D**) The lagging strand-enriched PCNA showed more PLA fluorescent spots with new H3 (GFP, 10.6 ± 1.4, n=21) than with old H3 (mKO, 6.5 ± 1.1, n=17), *: P< 0.05, based on Mann-Whitney U test.

Supplementary Tables:

Table S1: Quantification of histone H4 with imaging on fixed samples.

Pair #	Old H4 GSC/GB	New H4 GB/GSC	Pair #	Old H4 SG1/SG2	New H4 SG2/SG1
1	3.95	0.58	1	1.01	0.92
2	3.22	1.89	2	1.03	0.93
3	3.04	0.859	3	0.85	0.82
4	2.95	0.98	4	1.05	1.17
5	3.41	1.23	5	1.03	0.83
6	5.7	1.05	6	1.31	0.77
7	4.86	1.19	7	0.76	1.05
8	2.445	1.21	8	1.03	1.22
9	1.01	1.43	9	1.069	0.98
10	3.15	1.038	10	0.92	0.84
11	4.84	0.72	11	1.038	1.05
12	5.66	0.752	12	0.89	1.22
13	3.21	1.75	13	1.026	0.98
14	4.38	0.66	14	0.76	0.84
15	5.66	1.14	15	1.04	1.05
16	3.21	0.887	16	0.925	0.94
17	4.38	1.75	17	1.02	0.82
18	1.12	0.69	18	0.76	0.95
19	4.31	1.15	19	1.04	0.872
20	3.65	1.14	20	0.925	1.202
21	0.9	0.78	21	1.02	1.147
22	0.76	0.57	22	1.016	0.8
23	3.64	1.17	23	0.99	1.12
24	3.822	0.57	24	1.00	1.03

25	1.337	1.17	25	1.02	0.68
26	4.53	1.05	26	1.123	1.38
27	2.92	1.077	27	1.01	0.93
28	3.08	1.03			
29	0.94	1.287			
30	4.87	1.149			
31	5.97	2.116			
32	1.39	0.815			
33	0.98	0.982			

Table S2: Quantification of histone H2A with imaging on fixed samples.

Pair #	Old H2A GSC/GB	New H2A GB/GSC	Pair #	Old H2A SG1/SG2	New H2A SG2/SG1
1	0.975257657	0.98053122	1	1.088526265	1.043770558
2	0.968836869	0.966059723	2	1.016521777	1.016185595
3	0.969108816	0.941793393	3	0.94226273	0.974142098
4	1.232283465	1.633217284	4	1.067556671	0.915380396
5	1.025846378	1.041755268	5	1.009897937	0.962468942
6	1.053258093	0.999096786	6	1.042815974	0.946732867
7	0.96981108	1.186201719	7	1.019320953	0.950287833
8	0.797679181	1.357976654	8	1.222330968	0.885426578
9	1.075991617	1.122733612	9	0.995727661	1.019966875
10	1.121519519	0.901016184	10	0.930194711	1.009292519
11	1.061309268	1.103250478	11	0.931785196	0.931550686
12	0.91240285	1.066446402	12	0.986123708	0.979875209
13	0.801834862	1.204483553	13	0.925085483	1.045018182
14	1.070005651	0.987937274	14	1.019632679	1.10359635
15	0.72144534	1.247089104	15	1.035048915	1.119932432
16	1.338405425	1.246516489	16	0.969548629	0.972565036
17	0.898969072	1.154507556	17	0.972673954	1.035350772
18	1.152941753	1.019673558	18	1.023154848	1.16412729
19	1.054371002	0.823608964	19	0.978854429	1.153198983
20	0.920813893	1.027300496	20	1.055423123	1.029364311

Table S3: Quantification of histone H2B with imaging on fixed samples.

Pair #	Old H2B GSC/GB	New H2B GB/GSC	Pair #	Old H2B SG1/SG2	New H2B SG2/SG1
1	0.815283172	1.149883726	1	1.06879687	1.036802671
2	0.910809049	1.087101455	2	0.83419399	1.01759456
3	0.992565434	0.900208136	3	1.010622669	0.861117493
4	0.978807685	1.061501775	4	1.046838138	1.052032321
5	1.17406494	0.821823967	5	0.916185819	0.874832476
6	0.872269007	1.360653409	6	0.973981549	1.326719124
7	1.162729831	0.827364081	7	1.220158888	0.749905276
8	1.171490593	1.601112878	8	1.009274627	0.968346435
9	1.037883808	0.917360074	9	0.947504382	1.170238975
10	0.99783673	0.923628319	10	0.854147825	1.174910873
11	0.895076097	1.281920327	11	1.172142501	0.858156863
12	0.959500446	1.479566305	12	1.083404453	0.845157357
13	1.231086253	1.127473807	13	1.07626037	0.923235726
14	0.808704809	1.211914894	14	1.021646558	0.920400153
15	1.046689113	1.143965517	15	0.86262317	1.172370089
16	0.849082443	1.453828829	16	1.026491198	1.939485628
17	1.055365474	1.121270452	17	1.0234375	0.972416813
18	1.014446228	1.165391969	18	0.928342031	0.856763926
19	0.912596963	1.306268241	19	0.900293686	1.918833044
20	1.021970333	0.862912736	20	1.066753078	1.144069104
21	1.202621287	1.191425723	21	1.099325769	0.662652053
22	0.887726959	2.07110666	22	1.153474545	0.59781155
23	0.990796476	0.885693395	23	0.982679645	1.374321095
24	0.918245383	0.891502847	24	0.844495944	1.205987906
25	0.912221729	1.384310526	25	1.036036036	0.852305896
26	0.869454545	1.11416998	26	1.064761181	0.948237664
27	1.190698579	1.019536742	27	0.88406336	1.059149083
28	0.891282778	1.129701061	28	1.093008455	0.998295745
29	1.048793662	0.94980315	29	1.080438985	1.300522734
30	1.214413768	0.848577475	30	1.222637781	1.0442979
31	0.935564854	1.327795976	31	1.037889226	1.10251344
32	0.843987298	1.593786228	32	1.126153435	0.977582529
33	1.011382114	1.166823456	33	0.813552882	0.91765286
34	0.907251972	1.466248278	34	1.083184342	0.968471789
35	0.894008235	1.033427164	35	0.904325323	1.031899183
36	1.110156314	1.905524681	36	1.015971606	1.013173653
37	0.917364991	1.476244026			

38	0.964285714	1.280842528			
39	0.976632851	2.048527984			
40	0.96929659	0.890530557			

Table S4: Quantification of histone H1 with imaging on fixed samples.

Pair#	Old H1 GSC/GB	New H1 GB/GSC
1	1.231616	1.236307
2	1.313828	1.371778
3	1.280991	1.288979
4	2.686801	2.020878
5	1.214697	0.676174
6	0.960562	0.990234
7	1.147011	1.705283
8	1.629132	1.252325
9	0.67269	0.772935
10	0.846208	0.757713
11	1.223122	1.269666
12	0.903526	0.828135

Supplementary References:

Hime, G.R., Brill, J.A., and Fuller, M.T. (1996). Assembly of ring canals in the male germ line from structural components of the contractile ring. J Cell Sci *109 (Pt 12)*, 2779-2788.
Kolb, H.C., Finn, M.G., and Sharpless, K.B. (2001). Click Chemistry: Diverse Chemical Function from a Few Good Reactions. Angew Chem Int Ed Engl *40*, 2004-2021.
Moses, J.E., and Moorhouse, A.D. (2007). The growing applications of click chemistry. Chemical Society reviews *36*, 1249-1262.
Tran, V., Lim, C., Xie, J., and Chen, X. (2012). Asymmetric division of Drosophila male germline stem cell shows asymmetric histone distribution. Science *338*, 679-682.
Van Doren, M., Williamson, A.L., and Lehmann, R. (1998). Regulation of zygotic gene expression in Drosophila primordial germ cells. Curr Biol *8*, 243-246.